
Failure Modes of Variational Autoencoders and Their Effects on Downstream Tasks

Yaniv Yacoby, Weiwei Pan, Finale Doshi-Velez

John A. Paulson School of Engineering and Applied Sciences

Harvard University

Cambridge, MA 02138

{yanivyacoby, weiweipan}@g.harvard.edu, finale@seas.harvard.edu

Abstract

Variational Auto-encoders (VAEs) are deep generative latent variable models that are widely used for a number of downstream tasks. While it has been demonstrated that VAE training can suffer from a number of pathologies, existing literature lacks characterizations of exactly *when* these pathologies occur and *how* they impact down-stream task performance. In this paper we concretely characterize conditions under which VAE training exhibits pathologies and connect these failure modes to undesirable effects on specific downstream tasks, such as learning compressed and disentangled representations, adversarial robustness and semi-supervised learning.

1 Introduction

Variational Auto-encoders (VAEs) are deep generative latent variable models that transform simple distributions over a latent space to model complex data distributions [26]. They have been used for a wide range of downstream tasks, including: generating realistic looking synthetic data (e.g. [38]), learning compressed representations (e.g. [35, 14, 2]), adversarial defense using de-noising [32, 13], and, when expert knowledge is available, generating counter-factual data using weak or semi-supervision (e.g. [24, 45, 27]). Variational auto-encoders are widely used by practitioners due to the ease of their implementation and simplicity of their training. In particular, the common choice of mean-field Gaussian (MFG) approximate posteriors for VAEs (MFG-VAE) results an inference procedure that is straight-forward to implement and stable in training.

Unfortunately, a growing body of work has demonstrated that MFG-VAEs suffer from a variety of pathologies, including learning un-informative latent codes (e.g. [51, 21]) and unrealistic data distributions (e.g. [49]). When the data consists of images or text, rather than evaluating the model based on metrics alone, we often rely on “gut checks” to make sure that the quality of the latent representations the model learns and the synthetic data (as well as counterfactual data) generated by the model is high (e.g. by reading generate text or inspecting generated images visually [5, 27]). However, as VAEs are increasingly being used in application where the data is numeric, e.g. in medical or financial domains [37, 20, 52], these intuitive qualitative checks no longer apply. For example, in many medical applications, the original data features themselves (e.g. biometric reading) are difficult to analyze by human experts in raw form. In these cases, where the application touches human lives and potential model error/pathologies are particularly consequential, we need to have a clear theoretical understanding of the failure modes of our models as well as the potential negative consequences on down-stream tasks.

Recent work [54] attributes a number of the pathologies of MFG-VAEs to properties of the training objective; in particular, the objective may compromise learning a good generative model in order to

learn a good inference model – in other words, the inference model over-regularizes the generative model. While this pathology has been noted in literature [4, 55, 6], no prior work has characterized the *conditions* under which the MFG-VAE objective compromises learning a good generative model in order to learn a good inference model; moreover, no prior work has related MFG-VAE pathologies with the performance on *downstream tasks*. Rather, existing literature focuses on mitigating the regularizing effect of the inference model on the VAE generative model by using richer variational families (e.g. [25, 36, 33]). While promising, these methods introduce potentially significant additional computational costs to training, as well as new training issues (e.g. noisy gradients [41, 50, 39]). As such, it is important to understand precisely when MFG-VAEs exhibit pathologies and when alternative training methods are worth the computational trade-off. In this paper, we characterize the conditions under which MFG-VAEs perform poorly and link these failures to effects on a range of downstream tasks. While we might expect that methods designed to mitigate VAE training pathologies (e.g. methods with richer variational families [25]), will also alleviate the negative downstream effects, we find that this is not always so. Our observations point to reasons for further studying the performance VAE alternatives in these applications. Our contributions are both theoretical and empirical:

I. *When VAE pathologies occur*: (1) We characterize concrete conditions under which learning the inference model will compromise learning the generative model for MFG-VAEs. More problematically, we show that these bad solutions are *globally optimal* for the training objective, the ELBO. (2) We demonstrate that using the ELBO to select the output noise variance and the latent dimension results in biased estimates. (3) We propose synthetic data-sets that trigger these two pathologies and can be used to test future proposed inference methods.

II. *Effects on tasks*: (4) We demonstrate ways in which these pathologies affect key downstream tasks, including learning compressed, disentangled representations, adversarial robustness and semi-supervised learning. In semi-supervised learning, we are the first to document the instance of “functional collapse”, in which the data conditionals problematically collapse to the same distribution. (5) Lastly, we show that while the use of richer variational families alleviate VAE pathologies on unsupervised learning tasks, they introduce new ones in the semi-supervised tasks.

These contributions help identify when MFG-VAEs suffice, and when advanced methods are needed.

2 Related Work

Existing works that characterize MFG-VAEs pathologies largely focus on relating *local optima* of the training objective to a single pathology: the un-informativeness of the learned latent codes (posterior collapse) [15, 31, 9]. In contrast, there has been little work to characterize pathologies at the *global optima* of the MFG-VAE’s training objective. [54] shows that, when the decoder’s capacity is restricted, posterior collapse and the mismatch between aggregated posterior and prior can occur as global optima of the training objective. In contrast, we focus on *global optima* of the MFG-VAE objective in *fully general* settings: with fully flexible generative and inference models, as well as with and without learned observation noise.

Previous works (e.g. [54]) have connected VAE pathologies like posterior collapse to the over-regularizing effect of the variational family on the generative model. However while there are many works that mitigate the over-regularization issue (e.g. [4, 55, 6, 44]), none have given a full characterization of *when* the learned generative model is over-regularized, nor have they related the quality of the learned model to its performance on *down-stream tasks*. In particular, these works have shown that their proposed methods have higher test log-likelihood relative to a MFG-VAEs, but as we show in this paper, high test log-likelihood is not the only property needed for good performance on downstream tasks. Lastly, these works all propose fixes that require a potentially significant computational overhead. For instance, works that use complex variational families, such as normalizing flows [25], require a significant number of parameters to scale [23]. In the case of the Importance Weighted Autoencoder (IWAE) objective [4], which can be interpreted as having a more complex variational family [7], the complexity of the posterior scales with the number of importance samples used. Lastly, works that de-bias existing bounds [36, 33] all require several evaluations of the objective.

Given that MFG-VAEs remain popular today due to the ease of their implementation, speed of training, and their theoretical connections to other dimensionality reduction approaches like probabilistic

PCA [42, 8, 31], it is important to characterize the training pathologies of MFG-VAE, as well as the concrete connections between these pathologies and down-stream tasks. More importantly, this characterization will help clarify for which tasks and datasets a MFG-VAE suffices and for which the computational tradeoffs are worth it.

3 Background

Unsupervised VAEs [26] A VAE assumes the following generative process:

$$p(z) = \mathcal{N}(0, I), \quad p_\theta(x|z) = \mathcal{N}(f_\theta(z), \sigma_\epsilon^2 \cdot I) \quad (1)$$

where x in \mathbb{R}^D , $z \in \mathbb{R}^K$ is a latent variable and f_θ is a neural network parametrized by θ . We learn the likelihood parameters θ while jointly approximating the posterior $p_\theta(z|x)$ with $q_\phi(z|x)$:

$$\max_{\theta} \mathbb{E}_{p(x)} [\log p_\theta(x)] \geq \max_{\theta, \phi} \mathbb{E}_{p(x)} \left[\mathbb{E}_{q_\phi(z|x)} \left[\log \frac{p_\theta(x|z)p(z)}{q_\phi(z|x)} \right] \right] = \text{ELBO}(\theta, \phi) \quad (2)$$

where $p(x)$ is the true data distribution, $p_\theta(x)$ is the learned data distribution, and $q_\phi(z|x)$ is a MFG with mean and variance $\mu_\phi(x)$, $\sigma_\phi^2(x)$, parameterized by neural network with parameters ϕ . The VAE ELBO can alternately be written as a sum of two objectives – the “MLE objective” (MLEO), which maximizes the $p_\theta(x)$, and the “posterior matching objective” (PMO), which encourages variational posteriors to match posteriors of the generative model. That is, we can write:

$$\text{argmin}_{\theta, \phi} -\text{ELBO}(\theta, \phi) = \text{argmin}_{\theta, \phi} \underbrace{(D_{\text{KL}}[p(x)||p_\theta(x)])}_{\text{MLEO}} + \underbrace{\mathbb{E}_{p(x)} [D_{\text{KL}}[q_\phi(z|x)||p_\theta(z|x)]]}_{\text{PMO}} \quad (3)$$

This decomposition allows for a more intuitive interpretation of VAE training and illustrates the tension between approximating the true posteriors and approximating $p(x)$.

Semi-Supervised VAEs We extend the VAE model and inference to incorporate partial labels, allowing for some supervision of the latent space dimensions. For this, we use the semi-supervised model introduced by [24] as the “M2 model”, which assumes the generative process,

$$z \sim \mathcal{N}(0, I), \quad \epsilon \sim \mathcal{N}(0, \sigma_\epsilon^2 \cdot I), \quad y \sim p(y), \quad x|y, z = f_\theta(y, z) + \epsilon \quad (4)$$

where y is observed only a portion of the time. The inference objective for this model is typically written as a sum of three objectives, a lower bound for the likelihood of M labeled observations, a lower bound for the likelihood for N unlabeled observations, and a term encouraging the discriminative powers of the variational posterior:

$$\mathcal{J}(\theta, \phi) = \sum_{n=1}^N \mathcal{U}(x_n; \theta, \phi) + \gamma \cdot \sum_{m=1}^M \mathcal{L}(x_m, y_m; \theta, \phi) + \alpha \cdot \sum_{m=1}^M \log q_\phi(y_m|x_m) \quad (5)$$

where the \mathcal{U} and \mathcal{L} lower bound $p_\theta(x)$ and $p_\theta(x, y)$, respectively (see Appendix A); the last term in the sum is included to explicitly increase discriminative power of the posteriors $q_\phi(y_m|x_m)$ [24, 46]; α , γ controls the relative weights of the last two terms. Note that $\mathcal{J}(\theta, \phi)$ is only a lower bound of the observed data log-likelihood only when $\gamma = 1, \alpha = 0$, but in practice, γ, α are tuned as hyper-parameters. Following [24], we assume a MFG variational family for each of the unlabeled and labeled objectives.

4 When VAEs Fail: Pathologies of the VAE Objective

Our first set of contributions characterizes *when* MFG-VAEs fail. In Section 4.1, we identify two pathological properties of the VAE training objective. In Section 4.2 we introduce new synthetic benchmarks that demonstrate these pathologies and can be used to test future inference algorithms.

4.1 Formalizing Pathologies of the VAE Objective

We fix a set of realizable likelihood functions \mathcal{F} , implied by our choice of the generative model network architecture. We assume that \mathcal{F} is expressive enough to contain any smooth function, including the ground truth generating function.

When VAEs Fail I: The ELBO trades off generative model quality for simple posteriors Intuitively, global optima of the ELBO correspond to incorrect generative models under two conditions: (1) the true posterior is difficult to approximate by a MFG for a large portion of x 's, and (2) there does not exist a likelihood function f_θ in \mathcal{F} with a simpler posterior that approximates $p(x)$ well.

We formalize these intuitive conditions (1) and (2) in the theorem below. First, recall the decomposition the negative ELBO in Equation 3. In this discussion, we always set ϕ to be optimal for our choice of θ . Assuming that $p(x)$ is continuous, then for any $\eta \in \mathbb{R}$, we can decompose the PMO as:

$$\begin{aligned} \mathbb{E}_{p(x)} [D_{\text{KL}}[q_\phi(z|x)||p_\theta(z|x)]] = & \Pr[\mathcal{X}_{\text{Lo}}(\theta)] \mathbb{E}_{p(x)|\mathcal{X}_{\text{Lo}}} [D_{\text{KL}}[q_\phi(z|x)||p_\theta(z|x)]] \\ & + \Pr[\mathcal{X}_{\text{Hi}}(\theta)] \mathbb{E}_{p(x)|\mathcal{X}_{\text{Hi}}} [D_{\text{KL}}[q_\phi(z|x)||p_\theta(z|x)]] \end{aligned} \quad (6)$$

where $D_{\text{KL}}[q_\phi(z|x)||p_\theta(z|x)] \leq \eta$ on $\mathcal{X}_{\text{Lo}}(\theta)$, $D_{\text{KL}}[q_\phi(z|x)||p_\theta(z|x)] > \eta$ on $\mathcal{X}_{\text{Hi}}(\theta)$, with $\mathcal{X}_i(\theta) \subseteq \mathcal{X}$; where $\mathbb{E}_{p(x)|\mathcal{X}_i}$ is the expectation over $p(x)$ restricted to $\mathcal{X}_i(\theta)$ and renormalized, and $\Pr[\mathcal{X}_i]$ is the probability of $\mathcal{X}_i(\theta)$ under $p(x)$. Let us denote the expectation in first term on the right hand side of Equation 6 as $D_{\text{Lo}}(\theta)$ and the expectation in the second term as $D_{\text{Hi}}(\theta)$.

Let $f_{\theta_{\text{GT}}} \in \mathcal{F}$ be the ground truth likelihood function, for which we may assume that the MLE objective (MLEO) term is zero. Now conditions (1) and (2) above may be rewritten more formally as:

Theorem 1. *Suppose that there is an $\eta \in \mathbb{R}$ such that $\Pr[\mathcal{X}_{\text{Hi}}(\theta_{\text{GT}})] D_{\text{Hi}}(\theta_{\text{GT}})$ is greater than $\Pr[\mathcal{X}_{\text{Lo}}(\theta_{\text{GT}})] D_{\text{Lo}}(\theta_{\text{GT}})$. Suppose the following two conditions: (1) [True posterior often difficult] there exist an $f_\theta \in \mathcal{F}$ with $D_{\text{Lo}}(\theta_{\text{GT}}) \geq D_{\text{Lo}}(\theta)$ and*

$$\Pr[\mathcal{X}_{\text{Hi}}(\theta_{\text{GT}})] (D_{\text{Hi}}(\theta_{\text{GT}}) - D_{\text{Lo}}(\theta_{\text{GT}})) > \Pr[\mathcal{X}_{\text{Hi}}(\theta)] D_{\text{Hi}}(\theta) + D_{\text{KL}}[p(x)||p_\theta(x)];$$

and (2) [No good, simpler alternative] that for no such $f_\theta \in \mathcal{F}$ is the MLEO $D_{\text{KL}}[p(x)||p_\theta(x)]$ equal to zero. Then at the global minima (θ^, ϕ^*) of the negative ELBO, the MLEO will be non-zero.*

Theorem 1 shows that under conditions (1) and (2) the ELBO can prefer learning likelihood functions f_θ that reconstruct $p(x)$ poorly, even when learning the ground truth likelihood is possible! While the proof is straightforward (Appendix B.1), it is non-trivial to show that the conditions (1) and (2) are satisfied on actual datasets - we do this in Section 4.2.

When VAEs Fail II: The ELBO biases learning of the observation noise variance In practice, the noise variance of the dataset is unknown and it is common to estimate the variance as a hyper-parameter. Here, we show that learning the variance of ϵ either via hyper-parameter search or via direct optimization of the ELBO can be biased.

Theorem 2. *For an observation set of size N , we have that*

$$\underset{\sigma_\epsilon^{(d)^2}}{\text{argmin}} -\text{ELBO}(\theta, \phi, \sigma_\epsilon^{(d)^2}) = \frac{1}{N} \sum_{n=1}^N \mathbb{E}_{q_\phi(z|x_n)} \left[(x_n^{(d)} - f_\theta(z)^{(d)})^2 \right]. \quad (7)$$

Proof in Appendix B.2. The above theorem shows that the variance σ_ϵ^2 that minimizes the negative ELBO depends on the approximate posterior $q_\phi(z|x)$, and thus even when the generative model is set to the ground-truth, the learned σ_ϵ^2 will not equal the ground truth noise variance if $q_\phi(z|x_n)$ are poor approximations of the true posterior. Certainly, when the learned generative model does not capture $p(x)$ (say, due to the conditions in Theorem 1), then the learned σ_ϵ^2 will again be biased.

Remark: While the pathologies in Theorems 1, 2 seem to depend on our choice of variational family, they are actually artifacts of the ELBO. There are objectives that use MFG families to obtain unbiased estimates of the ground truth generative model and σ_ϵ^2 [12].

4.2 Benchmarks to Demonstrate of VAE Training Pathologies

We provide novel benchmarks to demonstrate the pathologies described in Theorems 1 and 2. These benchmarks not only provide intuition for these failure modes, they can also serve as benchmarks for testing future VAE objectives and inference. Finally, while examples here are synthetic in order to provide intuition for general failures on down-stream tasks, in Section 6 we describe how each example corresponds to a class of real datasets on which VAEs can exhibit training pathologies.

Experimental setup To show that an observed failure is due to pathologies identified in Theorem 1, we verify that: (A) the learned models have simple posteriors for high mass regions where the ground

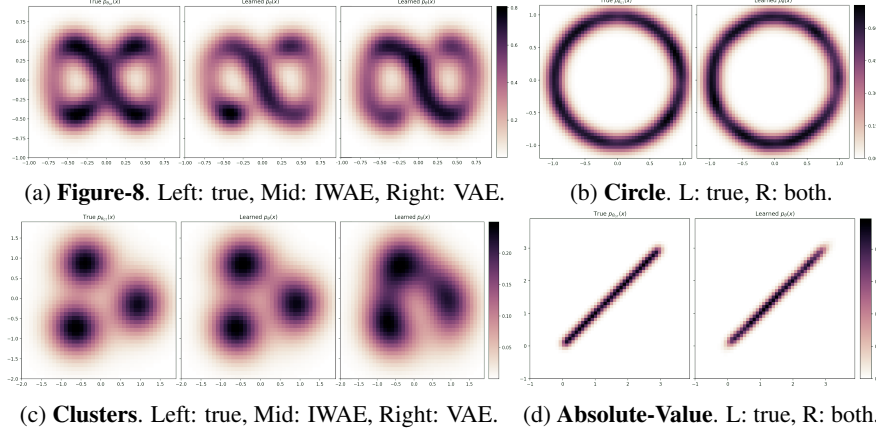


Figure 1: Comparison of true data distributions versus the corresponding learned distributions of VAE and IWAE. When conditions of Theorem 1 are satisfied, in examples (a) and (c), VAE training approximates $p(x)$ poorly and IWAE performs better. When one of the conditions is not met, in examples (b) and (d), then the VAE can learn $p(x)$ as well as IWAE.

truth models do not, (B) training with IWAE (complex variational families) results in generally superior generative models and (C) the VAE training cannot be improved meaningfully by methods designed to escape bad local optima, i.e. Lagging Inference Networks (LIN) [15]. We specifically chose IWAE as a baseline since we can easily control the complexity of the implied variational family using the number of importance samples S , and in doing so we encompass other types of variational families. We ensure that IWAE does not suffer from training issues (e.g. low signal-to-noise ratio) by ensuring $S \leq 20$ and by constructing all toy examples with 1D latent spaces.

We fix a flexible architecture (one that is significantly more expressive than needed to capture $f_{\theta_{\text{GT}}}$) so that our realizable set \mathcal{F} is diverse enough to include likelihoods with simpler posteriors. We train each model to reach global optima as follows: for each method and hyper-parameter settings, we train 5 random initialized randomly, and 5 random with the decoder and encoder initialized to ground truth values. We select the restart with the best value of the objective function. Details in Appendix C.

Benchmark: approximation of $p(x)$ is poor when Conditions (1) and (2) of Theorem 1 both hold. Consider the “Figure-8” Example in Figure 1a (described in Appendix F.1). For this dataset, values of z in $[-\infty, -3.0] \cup [3.0, \infty]$ map to similar values of x near $(0, 0)$, where $p(x)$ is high. We verify that, near $x = (0, 0)$, the posteriors $p_{\theta_{\text{GT}}}(z|x)$ are multi-modal, satisfying condition (1). We verify condition (2) is satisfied by considering all continuous parametrizations of the “Figure-8” curve: any such parametrization will result in a function f_{θ} for which distant values of z map to similar values near $(0, 0)$ and thus the posterior matching objective (PMO) will be high. As predicted by Theorem 1, the learned generative model approximates $p(x)$ poorly, learning posteriors that are simpler than those of the ground truth model.

To show that these issues occur because the MFG variational family over-regularizes the generative model, we compare VAE with LIN and IWAE. As expected, IWAE learns $p(x)$ better than LIN, which outperforms the VAE (Figure 1a). Like the VAE, LIN compromises learning the data distribution in order to learn simpler posteriors, since it also uses a MFG variational family. In contrast, IWAE is able to learn more complex posteriors and thus compromises $p(x)$ far less. However, note that with 20 importance samples, IWAE still does not learn $p(x)$ perfectly. See Appendix D.1 for a full quantitative analysis as well as more data-sets for which Theorem 1 holds. Next, we show that *both* conditions of Theorem 1 are necessary for the VAE training pathology to occur.

Benchmark: approximation of $p(x)$ may be fine when only condition (2) holds. What happens if the observations with highly non-Gaussian posterior were few in number? Consider the “Circle” Example in Figure 1b (described in Appendix F.2). Here, the regions that have non-Gaussian posteriors are near $x \approx (1.0, 0.0)$, since $z \in [-\infty, -3.0] \cup [3.0, \infty]$ map to points near $(1.0, 0.0)$. However, since the overall number of such points is small, the VAE objective does not trade-off capturing $p(x)$ for easy posterior approximation. Indeed, we see that VAE training is capable of recovering $p(x)$, regardless of whether training was initialized randomly or at the ground truth.

Benchmark: approximation of $p(x)$ may be fine when only condition (1) holds. We now study the case where the true posterior has a high PMO for a large portion of x 's, but there exist a f_θ in our realizable set \mathcal{F} that approximates $p(x)$ well and has simple posteriors. Consider the "Absolute-Value" Example visualized in Figure 1d. Although the posteriors under the ground truth generative model are complex, there is an alternative likelihood $f_\theta(z)$ that models $p(x)$ equally well and has simpler posteriors, and this is the model selected by the VAE objective, regardless of whether training was initialized randomly or at the ground truth. Details in Appendix F.3.

Benchmark: Theorem 2 implies that the ELBO biases noise variance estimates. Consider the "Spiral Dots" Example in Appendix F.5. We perform two experiments. In the first, we fix the noise variance ground-truth ($\sigma_\epsilon^2 = 0.01$), we initialize and train θ, ϕ following the experimental setup above, and finally, we recompute σ_ϵ^2 that maximizes the ELBO for the learned θ, ϕ . In the second experiment, we do the same, but train the ELBO jointly over $\sigma_\epsilon^2, \theta$ and ϕ . Using these two methods of learning the noise, we get 0.014 ± 0.001 and 0.020 ± 0.003 , respectively. The ELBO therefore over-estimates the noise variance by 50% and 100%, respectively.

5 Impact of Pathologies on Downstream Tasks

In Section 4, we described *when* VAE pathologies occur, both theoretically and through new benchmarks. Now, we describe how these pathologies can negatively impact specific downstream tasks. On unsupervised tasks, we show that IWAE can avoid the negative effects associated with the MFG variational family over-regularizing the generative model, while LIN cannot. However, surprisingly, IWAE cannot outperform the VAE on our semi-supervised tasks as its complex variational family allows the generative model to overfit.

Experiment Setup On unsupervised tasks, we consider only synthetic data, since existing work shows that on real data IWAE learns generative models with higher log data likelihood [25, 7]. For our semi-supervised tasks, we consider both synthetic data as well as 3 UCI data-sets: Diabetic Retinopathy Debrecen [3], Contraceptive Method Choice [1, 11] and the Titanic [1, 47] datasets. In these, we treat the outcome as a partially observed label (observed 10% of the time). These datasets are selected because their classification is hard, and as we will show here, this is the regime in which we expect semi-supervised VAE training to struggle.

5.1 Effects on Unsupervised Downstream Tasks

Disentangled Representations: Failure due to Theorem 1 In disentangled representation learning, we suppose that each dimension of the latent space corresponds to a task-meaningful concept [40, 5]. Our goal is to infer these meaningful ground truth latent dimensions. It's been noted in literature that this inference problem is ill-posed - that is, there are an infinite number of likelihood functions (and hence latent codes) that can capture $p(x)$ equally well [30]. In Appendix D.2, we show that, more problematically, the VAE objective can *prefer* learning the representations that *entangles* the ground-truth latent dimensions due to the pathology in Theorem 1.

Compressed Representations: Failure due to Theorem 1 In practice, if the task does not require a specific latent space dimensionality, K , one chooses a K that maximizes the $\log p_\theta(x)$. In Appendix D.3, we show that using a larger K and a smaller σ_ϵ^2 means we can capture the data distribution with a simpler function $f_\theta(z)$ and hence get simpler posteriors. That is, increasing K alleviates the need to compromise the generative model in order to improve the inference model and leads to better approximation of $p(x)$. Thus, the ELBO will favor model mismatch (K larger than the ground truth) and prevent us from learning highly compressed representations when they are available. We provide two examples where the ELBO prefers models with larger K over the ground truth model ($K = 1$), and that as K increases, the average informativeness of each latent code decreases, since the latent space learns to generate the observation noise ϵ . We confirm that the posteriors become simpler as K increases, lessening the incentive for the VAE to compromise on approximating $p(x)$. Also, while LIN also shows preference for higher K 's, IWAE does not.

Defenses against adversarial perturbations: Failure due to Theorems 1 and 2 Manifold-based defenses against adversarial attacks (e.g. [17, 34, 43, 16, 19]) require both accurate estimates of the noise as well as of the intrinsic dimensionality of the data (i.e. the ground truth latent dimensionality); however, Theorem 2 shows that the ELBO is unable to identify the correct σ_ϵ^2 at correct latent

dimensionality K , and incorrect compression (above, due to Theorem 1) may further result in incorrect noise estimates due to incorrect ground truth latent space dimensionality. See Appendix E for full analysis.

5.2 Effects on Semi-Supervised Downstream Tasks

In semi-supervised VAEs, we assume that some observations x have an additional label y [24]. These VAEs have been used for tasks such as generating synthetic cohorts (sampling from $p(x|y = 1)$, $p(x|y = 0)$ respectively), and for generating counterfactuals (generating a synthetic data x' with label $y = 0$ that is similar to a real observation x with $y = 1$). For these tasks, it is important to accurately model the data conditional $p(x|y)$. Surprisingly, Theorem 1 leads to a negative effect specific to semi-supervised tasks, a phenomenon we call “functional collapse”: the model ignores the partial labels given by the semi-supervision, causing the learned conditionals to collapse onto a single distribution, $p_\theta(x) \approx p_\theta(x|y = 0) \approx p_\theta(x|y = 1)$. While one might expect methods like IWAE to fix this issue, IWAE actually overfits to the few partial labels due to its rich variational family, causing it to perform no better than a MFG-VAE. In this section, we characterize *when* functional collapse occurs, as well as *how* it impacts semi-supervised downstream tasks.

Due to Functional Collapse, VAEs trade-off between generating realistic data and realistic counterfactuals In real datasets, we often have samples from multiple cohorts of the population. General characteristics of the population hold for all cohorts, but each cohort may have different distributions of these characteristics [28]. Formally, this means that all of the cohorts to lie on a shared manifold but each has a different distribution on that manifold (that is $x|y = 0$ and $x|y = 1$ lie on the same manifold but $p(x|y = 0) \neq p(x|y = 1)$). On such data, the ground truth model’s posterior for the unlabeled data $p_{\theta_{\text{GT}}}(z|x) = \int_y p_{\theta_{\text{GT}}}(z, y|x) dy$ will be multi-modal, since for each value of y there are a number of different likely z ’s, each from a different cohort. As such, using a MFG variational family for the unlabeled portion of the semi-supervised objective (\mathcal{U} in Equation 9) will encourage inference to either compromise learning the data-distribution in order to better approximate the posterior, or to learn the data distribution well but approximate the posterior poorly, depending on our prioritization of the two objectives (indicated by our the choice of the hyperparameter γ in Equation 9). In the first case, data generation will be compromised because the model will overfit to the partial labels; however the model will at least be able to generate from two distinct data conditionals $p(x|y = 0)$ and $p(x|y = 1)$. In contrast, in the latter case the learned model will be able to generate realistic data but not realistic cohorts since the model will over-regularize the likelihood function $f_\theta(z, y)$ to collapse to the same function for all values of y (functional collapse), thereby collapsing the data conditionals $p_\theta(x|y) \approx p_\theta(x)$. That is, $p_\theta(x|y)$ will generate identical looking cohort regardless of our choice of y .

We empirically demonstrate the trade-off between realistic data and realistic counterfactuals generation on the “Discrete Semi-Circle” Example in Figure 2g (full details in Appendix G.1). In this data-set, we show that the MFG-VAE is able to learn the data manifold and distribution well. However, the training objectives learn a model with a simple posterior (in comparison to the true posterior), causing the learned $f_\theta(z, y)$ to collapse to the same function for all values of y (Figure 2c vs. 2a). As a result, $p_\theta(x|y) \approx p_\theta(x)$ under the learned model. As expected, functional collapse occurs when training with LIN as well. In contrast, IWAE is able to learn two distinct data conditionals $p_\theta(x|y = 0)$, $p_\theta(x|y = 1)$, but it does so at a cost. ***IWAE does not regularize the generative model, and thus overfits to the few partial labels*** (Figure 2b). Lastly, IWAE learns $p(x)$ considerably worse than the VAE, while learning $p(x|y)$ significantly better. In Appendix D.4, we provide a full quantitative and qualitative analysis of the above on synthetic and real datasets. We also demonstrate an additional pathology for the case where y is continuous, in which a naive choice of the discriminator $q_\phi(y|x)$ causes functional collapse even in IWAE.

6 Implications for Practice

In this paper, we have presented two sets of contributions that advance our fundamental understanding of VAEs: first, we described the theory of *when* pathologies occur and introduced benchmarks to expose them, second, we described the *impact* of these pathologies on common downstream tasks. Now, we connect these insights with implications for using VAEs in practice.

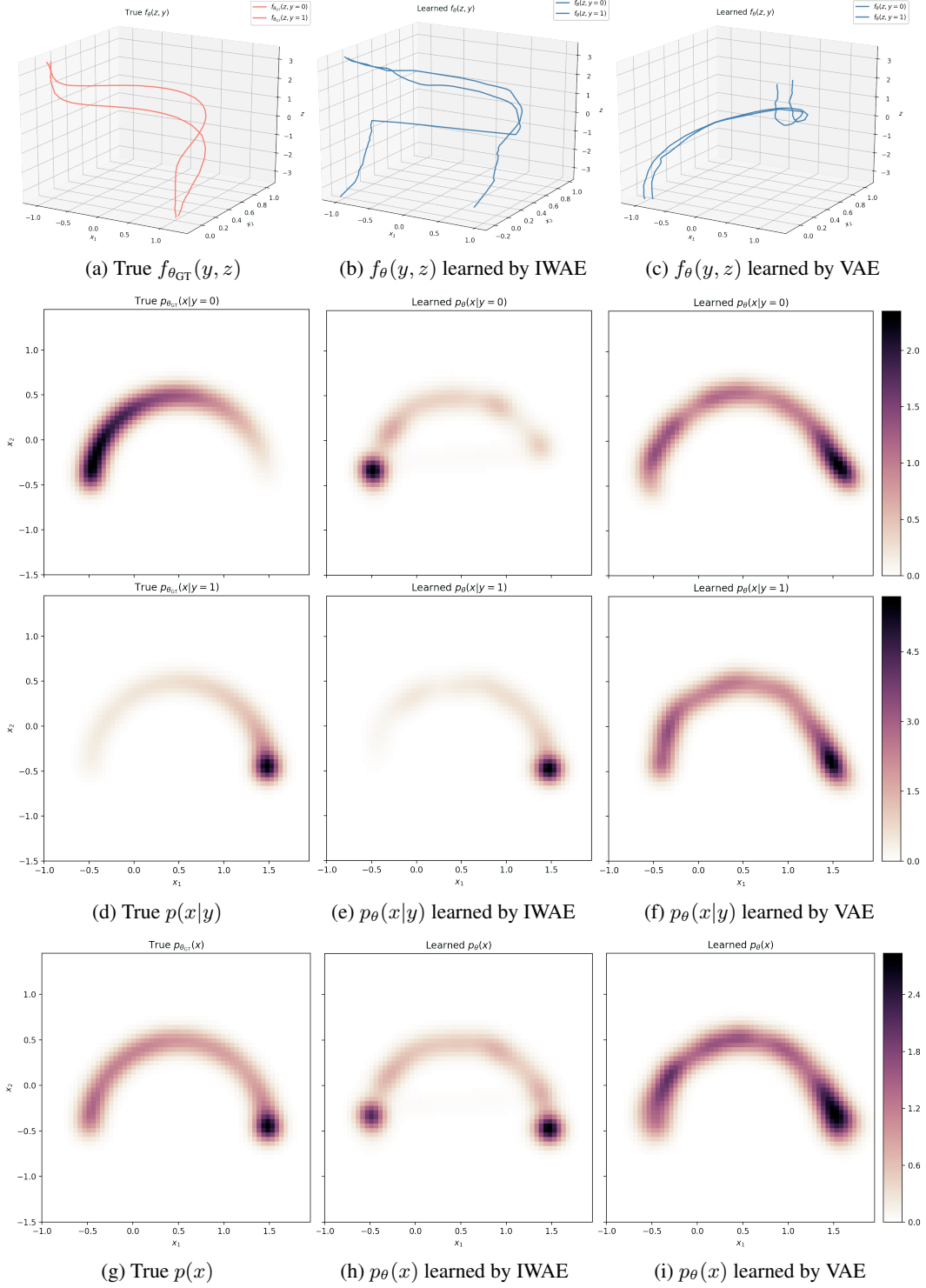


Figure 2: Discrete Semi-Circle. Comparison of VAE and IWAE on a semi-supervised example (left column: true, middle column: IWAE, right-column: VAE). The ground truth likelihood function $f_{\theta_{\text{GT}}}(y, z)$ shows two distinct functions, one for each $y = 0, 1$. The VAE’s $f_{\theta}(y, z)$ is over-regularized by a MFG variational family and learns two nearly identical functions (“functional collapse”). The IWAE’s $f_{\theta}(y, z)$ function is un-regularized and learns two distinct but overfitted functions. As a result, both the VAE and IWAE fail to learn $p(x)$ and $p(x|y)$. The VAE learns $p(x)$ better while IWAE learns $p(x|y)$ better.

How MFG-VAE training pathologies manifest in many real datasets. Our previous empirical demonstration of the pathology in Theorem 1 are synthetic; here we describe how the conditions of Theorem 1 can manifest in real datasets. The “Figure-8” Example in Figure 1a generalizes to any data manifold with high curvature (e.g. images from videos showing continuous physical transformations of objects), i.e. where the Euclidean distance between two points in a high density region on manifold is (A) less than the length of the geodesic connecting these points and (B) within 2 standard deviation of observation noise. The “Clusters” Example in Figure 1c generalizes to cases where we are learning low-dimensional representations of multimodal data distributions (e.g. popular image datasets where similar images lie in clusters). On these datasets, the VAE training objective would prefer compromising the quality of the generative model for posteriors that are easy to approximate. For the pathology noted in Theorem 2, we expect that the ELBO yields biased estimates of the observation noise whenever the learned model approximates $p(x)$ poorly. Finally, we expect the MFG-VAE’s performance on semi-supervised downstream tasks to suffer when a neural network is unable to accurately predict $y|x$. Difficulty in training a good classifier indicates that $x|y = 0$ and $x|y = 1$ lie roughly on the same manifold, and are difficult to distinguish, leading to the pathologies described in Section 5.2.

How to make inference choices We make three simple guidelines for practitioners when using VAEs in order to avoid the pathologies described in this work. While the guidelines are simple, our work provides formal rationales for *why* these practices matter (and we note that these best practices are not always used - e.g. it is common to set $\sigma_\epsilon^2 = 1$ without examining the data-set, or to learn it by optimizing jointly with model parameters [31]). Finally, as others have noted [12], a single methodological innovation is unlikely to fix all issues – each innovation makes a specific tradeoff; thus, improvements will need to be task/data specific. Our guidelines are: (1) Set the noise variance σ_ϵ^2 using domain expertise, or by hyper-parameter selection with an unbiased low-variance log-likelihood estimator. (2) Investigate the topology of the data (e.g. using topological data analysis, dimensionality reduction) before choosing a variational family. If the data lies on a manifold in distorted Euclidean space (e.g. “Figure-8” Example), or if the data is clustered (e.g. “Clusters” Example), use a rich variational family if you need to learn a very low-dimensional latent space. (3) Whenever using a rich variational family, apply regularization (e.g. ℓ_2) to the decoder network weights to prevent overfitting. Lastly, (4) on semi-supervised tasks, use a rich variational family for $q_\phi(z|x)$ in the unlabeled data objective (\mathcal{U} in Equation 9) when a simple neural network predicts $y|x$ with low balanced-accuracy (and use a MFG variational family otherwise).

7 Conclusion

In this work we characterize conditions under which global optima of the MFG-VAE objective exhibit pathologies and connect these failure modes to undesirable effects on specific downstream tasks. We find that while performing inference with richer variational families (which increases training time) can alleviate these issue on unsupervised tasks, the use of complex variational families introduce unexpected new pathologies in semi-supervised settings. Finally, we provide a set of synthetic datasets on which MFG-VAE exhibits pathologies. We hope that these examples contribute to a benchmarking dataset of “edge-cases” to test future VAE models and inference methods.

Acknowledgments

WP acknowledges support from the Harvard Institute of Applied Computational Sciences. YY acknowledges support from NIH 5T32LM012411-04 and from the IBM Faculty Research Award.

References

- [1] Jesus Alcala-Fdez, Alberto Fernández, Julián Luengo, J. Derrac, S Garcia, Luciano Sanchez, and Francisco Herrera. Keel data-mining software tool: Data set repository, integration of algorithms and experimental analysis framework. *Journal of Multiple-Valued Logic and Soft Computing*, 17:255–287, 01 2010.
- [2] Alexander A. Alemi, Ben Poole, Ian Fischer, Joshua V. Dillon, Rif A. Saurous, and Kevin Murphy. Fixing a Broken ELBO. *arXiv e-prints*, page arXiv:1711.00464, November 2017.

- [3] Balint Antal and Andras Hajdu. An ensemble-based system for automatic screening of diabetic retinopathy. *arXiv e-prints*, page arXiv:1410.8576, October 2014.
- [4] Yuri Burda, Roger Grosse, and Ruslan Salakhutdinov. Importance Weighted Autoencoders. *arXiv:1509.00519 [cs, stat]*, November 2016. arXiv: 1509.00519.
- [5] Ricky T. Q. Chen, Xuechen Li, Roger Grosse, and David Duvenaud. Isolating Sources of Disentanglement in Variational Autoencoders. *arXiv e-prints*, page arXiv:1802.04942, February 2018.
- [6] Chris Cremer, Xuechen Li, and David Duvenaud. Inference Suboptimality in Variational Autoencoders. *arXiv:1801.03558 [cs, stat]*, May 2018. arXiv: 1801.03558.
- [7] Chris Cremer, Quaid Morris, and David Duvenaud. Reinterpreting Importance-Weighted Autoencoders. *arXiv:1704.02916 [stat]*, August 2017. arXiv: 1704.02916.
- [8] Bin Dai, Yu Wang, John Aston, Gang Hua, and David Wipf. Connections with Robust PCA and the Role of Emergent Sparsity in Variational Autoencoder Models. page 42.
- [9] Bin Dai, Ziyu Wang, and David Wipf. The Usual Suspects? Reassessing Blame for VAE Posterior Collapse. *arXiv e-prints*, page arXiv:1912.10702, December 2019.
- [10] Josip Djolonga and Andreas Krause. Learning Implicit Generative Models Using Differentiable Graph Tests. *arXiv e-prints*, page arXiv:1709.01006, Sep 2017.
- [11] Dheeru Dua and Casey Graff. UCI machine learning repository, 2017.
- [12] Axel Finke and Alexandre H. Thiery. On importance-weighted autoencoders. *arXiv:1907.10477 [cs, stat]*, September 2019. arXiv: 1907.10477 version: 2.
- [13] Partha Ghosh, Arpan Losalka, and Michael J Black. Resisting Adversarial Attacks using Gaussian Mixture Variational Autoencoders. *arXiv e-prints*, page arXiv:1806.00081, May 2018.
- [14] Karol Gregor, Frederic Besse, Danilo Jimenez Rezende, Ivo Danihelka, and Daan Wierstra. Towards conceptual compression. In D. D. Lee, M. Sugiyama, U. V. Luxburg, I. Guyon, and R. Garnett, editors, *Advances in Neural Information Processing Systems 29*, pages 3549–3557. Curran Associates, Inc., 2016.
- [15] Junxian He, Daniel Spokoyny, Graham Neubig, and Taylor Berg-Kirkpatrick. Lagging Inference Networks and Posterior Collapse in Variational Autoencoders. *arXiv:1901.05534 [cs, stat]*, January 2019. arXiv: 1901.05534.
- [16] Uiwon Hwang, Jaewoo Park, Hyemi Jang, Sungroh Yoon, and Nam Ik Cho. PuVAE: A Variational Autoencoder to Purify Adversarial Examples. *arXiv e-prints*, page arXiv:1903.00585, March 2019.
- [17] Ajil Jalal, Andrew Ilyas, Constantinos Daskalakis, and Alexandros G. Dimakis. The Robust Manifold Defense: Adversarial Training using Generative Models. *arXiv e-prints*, page arXiv:1712.09196, December 2017.
- [18] Eric Jang, Shixiang Gu, and Ben Poole. Categorical Reparameterization with Gumbel-Softmax. *arXiv e-prints*, page arXiv:1611.01144, November 2016.
- [19] Uyeong Jang, Somesh Jha, and Susmit Jha. ON THE NEED FOR TOPOLOGY-AWARE GENERATIVE MODELS FOR MANIFOLD-BASED DEFENSES. page 24, 2020.
- [20] Shalmali Joshi, Oluwasanmi Koyejo, Warut Vijitbenjaronk, Been Kim, and Joydeep Ghosh. Towards realistic individual recourse and actionable explanations in black-box decision making systems. *arXiv preprint arXiv:1907.09615*, 2019.
- [21] Yoon Kim, Sam Wiseman, Andrew C. Miller, David Sontag, and Alexander M. Rush. Semi-Amortized Variational Autoencoders. *arXiv e-prints*, page arXiv:1802.02550, February 2018.
- [22] Diederik P. Kingma and Jimmy Ba. Adam: A Method for Stochastic Optimization. *arXiv e-prints*, page arXiv:1412.6980, December 2014.
- [23] Diederik P. Kingma and Prafulla Dhariwal. Glow: Generative Flow with Invertible 1x1 Convolutions. *arXiv:1807.03039 [cs, stat]*, July 2018. arXiv: 1807.03039.
- [24] Diederik P. Kingma, Danilo J. Rezende, Shakir Mohamed, and Max Welling. Semi-Supervised Learning with Deep Generative Models. *arXiv e-prints*, page arXiv:1406.5298, June 2014.

- [25] Diederik P. Kingma, Tim Salimans, Rafal Jozefowicz, Xi Chen, Ilya Sutskever, and Max Welling. Improving Variational Inference with Inverse Autoregressive Flow. *arXiv e-prints*, page arXiv:1606.04934, June 2016.
- [26] Diederik P Kingma and Max Welling. Auto-Encoding Variational Bayes. *arXiv e-prints*, page arXiv:1312.6114, December 2013.
- [27] Jack Klys, Jake Snell, and Richard Zemel. Learning Latent Subspaces in Variational Autoencoders. *arXiv e-prints*, page arXiv:1812.06190, December 2018.
- [28] Jack Klys, Jake Snell, and Richard Zemel. Learning latent subspaces in variational autoencoders. In *Advances in Neural Information Processing Systems*, pages 6444–6454, 2018.
- [29] Alexander Kraskov, Harald Stögbauer, and Peter Grassberger. Estimating mutual information. 69(6):066138, June 2004.
- [30] Francesco Locatello, Stefan Bauer, Mario Lucic, Gunnar Rätsch, Sylvain Gelly, Bernhard Schölkopf, and Olivier Bachem. Challenging Common Assumptions in the Unsupervised Learning of Disentangled Representations. *arXiv e-prints*, page arXiv:1811.12359, November 2018.
- [31] James Lucas, George Tucker, Roger Grosse, and Mohammad Norouzi. Don’t Blame the ELBO! A Linear VAE Perspective on Posterior Collapse. *arXiv e-prints*, page arXiv:1911.02469, November 2019.
- [32] Yi Luo and Henry Pfister. Adversarial Defense of Image Classification Using a Variational Auto-Encoder. *arXiv e-prints*, page arXiv:1812.02891, December 2018.
- [33] Yucen Luo, Alex Beatson, Mohammad Norouzi, Jun Zhu, David Duvenaud, Ryan P. Adams, and Ricky T. Q. Chen. SUMO: Unbiased Estimation of Log Marginal Probability for Latent Variable Models. *arXiv:2004.00353 [cs, stat]*, April 2020. arXiv: 2004.00353.
- [34] Dongyu Meng and Hao Chen. MagNet: a Two-Pronged Defense against Adversarial Examples. *arXiv e-prints*, page arXiv:1705.09064, May 2017.
- [35] Yishu Miao and Phil Blunsom. Language as a Latent Variable: Discrete Generative Models for Sentence Compression. *arXiv e-prints*, page arXiv:1609.07317, September 2016.
- [36] Sebastian Nowozin. DEBIASING EVIDENCE APPROXIMATIONS: ON IMPORTANCE-WEIGHTED AUTOENCODERS AND JACKKNIFE VARIATIONAL INFERENCE. page 16, 2018.
- [37] Stephen Pfohl, Tony Duan, Daisy Yi Ding, and Nigam H Shah. Counterfactual reasoning for fair clinical risk prediction. *arXiv preprint arXiv:1907.06260*, 2019.
- [38] Yunchen Pu, Zhe Gan, Ricardo Henao, Xin Yuan, Chunyuan Li, Andrew Stevens, and Lawrence Carin. Variational autoencoder for deep learning of images, labels and captions. In D. D. Lee, M. Sugiyama, U. V. Luxburg, I. Guyon, and R. Garnett, editors, *Advances in Neural Information Processing Systems 29*, pages 2352–2360. Curran Associates, Inc., 2016.
- [39] Tom Rainforth, Adam R. Kosiorek, Tuan Anh Le, Chris J. Maddison, Maximilian Igl, Frank Wood, and Yee Whye Teh. Tighter Variational Bounds are Not Necessarily Better. *arXiv:1802.04537 [cs, stat]*, March 2019. arXiv: 1802.04537.
- [40] Karl Ridgeway. A Survey of Inductive Biases for Factorial Representation-Learning. *arXiv e-prints*, page arXiv:1612.05299, December 2016.
- [41] Geoffrey Roeder, Yuhuai Wu, and David Duvenaud. Sticking the Landing: Simple, Lower-Variance Gradient Estimators for Variational Inference. *arXiv e-prints*, page arXiv:1703.09194, March 2017.
- [42] Michal Rolínek, Dominik Zietlow, and Georg Martius. Variational Autoencoders Pursue PCA Directions (by Accident). *arXiv:1812.06775 [cs, stat]*, April 2019. arXiv: 1812.06775.
- [43] Pouya Samangouei, Maya Kabkab, and Rama Chellappa. Defense-GAN: Protecting Classifiers Against Adversarial Attacks Using Generative Models. *arXiv e-prints*, page arXiv:1805.06605, May 2018.
- [44] Rui Shu, Hung H Bui, Shengjia Zhao, Mykel J Kochenderfer, and Stefano Ermon. Amortized Inference Regularization. In S. Bengio, H. Wallach, H. Larochelle, K. Grauman, N. Cesa-Bianchi, and R. Garnett, editors, *Advances in Neural Information Processing Systems 31*, pages 4393–4402. Curran Associates, Inc., 2018.

- [45] N. Siddharth, Brooks Paige, Jan-Willem van de Meent, Alban Desmaison, Noah D. Goodman, Pushmeet Kohli, Frank Wood, and Philip H. S. Torr. Learning Disentangled Representations with Semi-Supervised Deep Generative Models. *arXiv:1706.00400 [cs, stat]*, November 2017. arXiv: 1706.00400.
- [46] N. Siddharth, Brooks Paige, Jan-Willem van de Meent, Alban Desmaison, Noah D. Goodman, Pushmeet Kohli, Frank Wood, and Philip H. S. Torr. Learning Disentangled Representations with Semi-Supervised Deep Generative Models. *arXiv e-prints*, page arXiv:1706.00400, June 2017.
- [47] Jeffrey Simonoff. The "unusual episode" and a second statistics course. *Journal of Statistics Education*, 5, 03 1997.
- [48] Lucas Theis, Aaron van den Oord, and Matthias Bethge. A note on the evaluation of generative models. *arXiv:1511.01844 [cs, stat]*, April 2016. arXiv: 1511.01844.
- [49] Jakub M. Tomczak and Max Welling. VAE with a VampPrior. *arXiv e-prints*, page arXiv:1705.07120, May 2017.
- [50] George Tucker, Dieterich Lawson, Shixiang Gu, and Chris J. Maddison. Doubly Reparameterized Gradient Estimators for Monte Carlo Objectives. *arXiv:1810.04152 [cs, stat]*, November 2018. arXiv: 1810.04152.
- [51] Aaron van den Oord, Oriol Vinyals, and Koray Kavukcuoglu. Neural Discrete Representation Learning. *arXiv e-prints*, page arXiv:1711.00937, November 2017.
- [52] Gregory P Way and Casey S Greene. Extracting a biologically relevant latent space from cancer transcriptomes with variational autoencoders. *BioRxiv*, page 174474, 2017.
- [53] Yuhuai Wu, Yuri Burda, Ruslan Salakhutdinov, and Roger Grosse. On the Quantitative Analysis of Decoder-Based Generative Models. *arXiv:1611.04273 [cs]*, June 2017. arXiv: 1611.04273.
- [54] Yaniv Yacoby, Weiwei Pan, and Finale Doshi-Velez. Characterizing and Avoiding Problematic Global Optima of Variational Autoencoders. *arXiv e-prints*, page arXiv:2003.07756, March 2020.
- [55] Shengjia Zhao, Jiaming Song, and Stefano Ermon. Towards Deeper Understanding of Variational Autoencoding Models. *arXiv:1702.08658 [cs, stat]*, February 2017. arXiv: 1702.08658.

Appendix

Table of Contents

A The Semi-Supervised VAE Training Objective	13
B Proofs of Theorems	14
B.1 Proof of Theorem 1	14
B.2 Proof of Theorem 2	15
C Experimental Details	15
D Quantitative Results	17
D.1 Approximation of $p(x)$ is poor when both conditions of Theorem 1 hold	17
D.2 Failure to Learn Disentangled Representations due to Theorem 1	17
D.3 VAE training pathologies hinder learning compressed representations due to Theorem 1	18
D.4 VAEs trade-off between generating realistic data and realistic counterfactuals in semi-supervision due to Theorem 1	18
E Defense Against Adversarial Perturbations Requires the True Observation Noise and Latent Dimensionality	20
F Unsupervised Pedagogical Examples	21
F.1 Figure-8 Example	21
F.2 Circle Example	21
F.3 Absolute-Value Example	22
F.4 Clusters Example	22
F.5 Spiral Dots Example	22
G Semi-Supervised Pedagogical Examples	23
G.1 Discrete Semi-Circle Example	23
G.2 Continuous Semi-Circle Example	23
H Qualitative Results	25
H.1 Qualitative results to support necessity of both conditions of Theorem 1	25
H.2 Qualitative Demonstration of Unsupervised VAE Pathologies	28
H.3 Qualitative Demonstration of Semi-Supervised VAE Pathologies	35
H.4 When learning compressed representations, posterior is simpler for mismatched models	41

A The Semi-Supervised VAE Training Objective

We extend VAE model and inference to incorporate partial labels, allowing for some supervision of the latent space dimensions. For this, we use the semi-supervised model first introduced by [24] as the “M2 model”. We assume the following generative process:

$$z \sim \mathcal{N}(0, I), \quad \epsilon \sim \mathcal{N}(0, \sigma_\epsilon^2 \cdot I), \quad y \sim p(y), \quad x|y, z = f_\theta(y, z) + \epsilon \quad (8)$$

where y is observed only a portion of the time. Inference objective for this model can be written as a sum of two objectives, a lower bound for the likelihood of M labeled observations and a lower bound for the likelihood for N unlabeled observations:

$$\mathcal{J}(\theta, \phi) = \sum_{n=1}^N \mathcal{U}(x_n; \theta, \phi) + \gamma \cdot \sum_{m=1}^M \mathcal{L}(x_m, y_m; \theta, \phi) \quad (9)$$

where \mathcal{U} and \mathcal{L} lower bound $p_\theta(x)$ and $p_\theta(x, y)$, respectively:

$$\log p_\theta(x, y) \geq \underbrace{\mathbb{E}_{q_\phi(z|x, y)} [-\log p_\theta(x|y, z)] - \log p(y) + D_{\text{KL}}[q_\phi(z|x, y)||p(z)]}_{\mathcal{L}(x, y; \theta, \phi)} \quad (10)$$

$$\log p_\theta(x) \geq \underbrace{\mathbb{E}_{q_\phi(y|x)q_\phi(z|x)} [-\log p_\theta(x|y, z)] + D_{\text{KL}}[q_\phi(y|x)||p(y)] + D_{\text{KL}}[q_\phi(z|x)||p(z)]}_{\mathcal{U}(x; \theta, \phi)} \quad (11)$$

and γ controls their relative weight (as done by [46]). When using IWAE, we substitute the IWAE lower bounds for \mathcal{U} and \mathcal{L} as follows:

$$\log p_\theta(x, y) \geq \underbrace{\mathbb{E}_{z_1, \dots, z_S \sim q_\phi(z|x, y)} \left[\log \frac{1}{S} \frac{p_\theta(x, y, z_s)}{q_\phi(z_s|x, y)} \right]}_{\mathcal{L}(x, y; \theta, \phi)} \quad (12)$$

$$\log p_\theta(x) \geq \underbrace{\mathbb{E}_{(y_1, z_1), \dots, (y_S, z_S) \sim q_\phi(y|x)q_\phi(z|x)} \left[\log \frac{1}{S} \sum_{s=1}^S \frac{p_\theta(x, y_s, z_s)}{q_\phi(y_s|x)q_\phi(z_s|x)} \right]}_{\mathcal{U}(x; \theta, \phi)} \quad (13)$$

B Proofs of Theorems

B.1 Proof of Theorem 1

Recall the decomposition the negative ELBO in Main Paper Equation 3. In the following discussion, we always set ϕ to be optimal for our choice of θ . Assuming that $p(x)$ is continuous, then for any $\eta \in \mathbb{R}$, we can further decompose the PMO:

$$\begin{aligned} \mathbb{E}_{p(x)} [D_{\text{KL}}[q_\phi(z|x)||p_\theta(z|x)]] &= \Pr[\mathcal{X}_{\text{Lo}}(\theta)] \mathbb{E}_{p(x)|\mathcal{X}_{\text{Lo}}} [D_{\text{KL}}[q_\phi(z|x)||p_\theta(z|x)]] \\ &\quad + \Pr[\mathcal{X}_{\text{Hi}}(\theta)] \mathbb{E}_{p(x)|\mathcal{X}_{\text{Hi}}} [D_{\text{KL}}[q_\phi(z|x)||p_\theta(z|x)]] \end{aligned} \quad (14)$$

where $D_{\text{KL}}[q_\phi(z|x)||p_\theta(z|x)] \leq \eta$ on $\mathcal{X}_{\text{Lo}}(\theta)$, $D_{\text{KL}}[q_\phi(z|x)||p_\theta(z|x)] > \eta$ on $\mathcal{X}_{\text{Hi}}(\theta)$, with $\mathcal{X}_i(\theta) \subseteq \mathcal{X}$; where $\mathbb{E}_{p(x)|\mathcal{X}_i}$ is the expectation over $p(x)$ restricted to $\mathcal{X}_i(\theta)$ and renormalized, and $\Pr[\mathcal{X}_i]$ is the probability of $\mathcal{X}_i(\theta)$ under $p(x)$. Let us denote the expectation in first term on the right hand side of Equation 14 as $D_{\text{Lo}}(\theta)$ and the expectation in the second term as $D_{\text{Hi}}(\theta)$.

Let $f_{\theta_{\text{GT}}} \in \mathcal{F}$ be the ground truth likelihood function, for which we may assume that the MLE objective (MLEO) term is zero. We can now state our claim:

Theorem. Suppose that there exist an $\eta \in \mathbb{R}$ such that $\Pr[\mathcal{X}_{\text{Hi}}(\theta_{\text{GT}})] D_{\text{Hi}}(\theta_{\text{GT}})$ is greater than $\Pr[\mathcal{X}_{\text{Lo}}(\theta_{\text{GT}})] D_{\text{Lo}}(\theta_{\text{GT}})$. Suppose that (1) there exist an $f_\theta \in \mathcal{F}$ such that $D_{\text{Lo}}(\theta_{\text{GT}}) \geq D_{\text{Lo}}(\theta)$ and

$$\Pr[\mathcal{X}_{\text{Hi}}(\theta_{\text{GT}})] (D_{\text{Hi}}(\theta_{\text{GT}}) - D_{\text{Lo}}(\theta_{\text{GT}})) > \Pr[\mathcal{X}_{\text{Hi}}(\theta)] D_{\text{Hi}}(\theta) + D_{\text{KL}}[p(x)||p_\theta(x)];$$

suppose also that (2) that for no such $f_\theta \in \mathcal{F}$ is the MLEO $D_{\text{KL}}[p(x)||p_\theta(x)]$ equal to zero. Then at the global minima (θ^*, ϕ^*) of the negative ELBO, the MLEO will be non-zero.

Proof. The proof is straightforward. Condition (1) of the theorem implies that the negative ELBO of f_θ will be lower than that of $f_{\theta_{\text{GT}}}$. That is, we can write:

$$-\text{ELBO}(\theta_{\text{GT}}, \phi_{\text{GT}}) = \Pr[\mathcal{X}_{\text{Hi}}(\theta_{\text{GT}})] D_{\text{Hi}}(\theta_{\text{GT}}) + \Pr[\mathcal{X}_{\text{Lo}}(\theta_{\text{GT}})] D_{\text{Lo}}(\theta_{\text{GT}}) \quad (15)$$

$$= \Pr[\mathcal{X}_{\text{Hi}}(\theta_{\text{GT}})] D_{\text{Hi}}(\theta_{\text{GT}}) + (1 - \Pr[\mathcal{X}_{\text{Hi}}(\theta_{\text{GT}})]) D_{\text{Lo}}(\theta_{\text{GT}}) \quad (16)$$

$$= \Pr[\mathcal{X}_{\text{Hi}}(\theta_{\text{GT}})] (D_{\text{Hi}}(\theta_{\text{GT}}) - D_{\text{Lo}}(\theta_{\text{GT}})) + D_{\text{Lo}}(\theta_{\text{GT}}) \quad (17)$$

$$> \underbrace{\Pr[\mathcal{X}_{\text{Hi}}(\theta)] D_{\text{Hi}}(\theta) + \Pr[\mathcal{X}_{\text{Lo}}(\theta)] D_{\text{Lo}}(\theta) + D_{\text{KL}}[p(x)||p_\theta(x)]}_{-\text{ELBO}(\theta, \phi)} \quad (18)$$

So we have that $-\text{ELBO}(\theta_{\text{GT}}, \phi_{\text{GT}}) > -\text{ELBO}(\theta, \phi)$. Note again that by construction ϕ_{GT} and ϕ are both optimal for θ_{GT} and θ , respectively.

Furthermore, if there is an $f_{\theta'} \in \mathcal{F}$ such that $-\text{ELBO}(\theta', \phi') < -\text{ELBO}(\theta, \phi)$, then it must also satisfy the conditions in assumption (1) and, hence, the global minima of the negative ELBO satisfy the conditions in assumption (2). By assumption (2), at the global minima of the negative ELBO, the MLEO $D_{\text{KL}}[p(x)||p_\theta(x)]$ cannot be equal to zero. \square

B.2 Proof of Theorem 2

In practice, the noise variance of the dataset is unknown and it is common to estimate the variance as a hyper-parameter. Here, we show that learning the variance of ϵ either via hyper-parameter search or via direct optimization of the ELBO can be biased.

Theorem. *For an observation set of size N , we have that*

$$\operatorname{argmin}_{\sigma_\epsilon^{(d)^2}} -\text{ELBO}(\theta, \phi, \sigma_\epsilon^{(d)^2}) = \frac{1}{N} \sum_{n=1}^N \mathbb{E}_{q_\phi(z|x_n)} \left[(x_n^{(d)} - f_\theta(z)^{(d)})^2 \right]. \quad (19)$$

Proof. We rewrite the negative ELBO:

$$\operatorname{argmin}_{\sigma_\epsilon^{(d)^2}} -\text{ELBO}(\theta, \phi, \sigma_\epsilon^{(d)^2}) \quad (20)$$

$$= \operatorname{argmin}_{\sigma_\epsilon^{(d)^2}} \mathbb{E}_{p(x)} \left[\mathbb{E}_{q_\phi(z|x)} [-\log p_\theta(x|z)] + D_{\text{KL}}[q_\phi(z|x)||p(z)] \right] \quad (21)$$

$$= \operatorname{argmin}_{\sigma_\epsilon^{(d)^2}} \mathbb{E}_{p(x)} \left[\mathbb{E}_{q_\phi(z|x)} [-\log p_\theta(x|z)] \right] \quad (22)$$

$$= \operatorname{argmin}_{\sigma_\epsilon^{(d)^2}} \mathbb{E}_{p(x)} \left[\mathbb{E}_{q_\phi(z|x)} \left[-\sum_{d=1}^D \log \left(\frac{1}{\sqrt{2\pi\sigma_\epsilon^{(d)^2}}} \cdot \exp \left(\frac{-(x^{(d)} - f_\theta(z)^{(d)})^2}{2\sigma_\epsilon^{(d)^2}} \right) \right) \right] \right] \quad (23)$$

$$= \operatorname{argmin}_{\sigma_\epsilon^{(d)^2}} \sum_{d=1}^D \mathbb{E}_{p(x)} \left[\mathbb{E}_{q_\phi(z|x)} \left[\log \left(\sqrt{2\pi\sigma_\epsilon^{(d)^2}} \right) + \frac{(x^{(d)} - f_\theta(z)^{(d)})^2}{2\sigma_\epsilon^{(d)^2}} \right] \right] \quad (24)$$

$$= \operatorname{argmin}_{\sigma_\epsilon^{(d)^2}} \sum_{d=1}^D \mathbb{E}_{p(x)} \left[\mathbb{E}_{q_\phi(z|x)} \left[\log \left(\sigma_\epsilon^{(d)} \right) + \frac{(x^{(d)} - f_\theta(z)^{(d)})^2}{2\sigma_\epsilon^{(d)^2}} \right] \right] \quad (25)$$

$$= \operatorname{argmin}_{\sigma_\epsilon^{(d)^2}} \sum_{d=1}^D \log \left(\sigma_\epsilon^{(d)} \right) + \frac{1}{2\sigma_\epsilon^{(d)^2}} \cdot \underbrace{\mathbb{E}_{p(x)} \left[\mathbb{E}_{q_\phi(z|x)} \left[(x^{(d)} - f_\theta(z)^{(d)})^2 \right] \right]}_{C(\theta, \phi, d)} \quad (26)$$

Setting the gradient of the above with respect to σ_ϵ^2 equal to zero yields the following:

$$0 = -\frac{\partial}{\partial \sigma_\epsilon^{(d)^2}} \text{ELBO}(\theta, \phi, \sigma_\epsilon^{(d)^2}) \quad (27)$$

$$= \frac{\sigma_\epsilon^{(d)^2} - C(\theta, \phi, d)}{\sigma_\epsilon^{(d)^3}}. \quad (28)$$

Thus, we can write,

$$\sigma_\epsilon^{(d)^2} = C(\theta, \phi, d) = \mathbb{E}_{p(x)} \left[\mathbb{E}_{q_\phi(z|x)} \left[(x^{(d)} - f_\theta(z)^{(d)})^2 \right] \right] \quad (29)$$

$$\approx \frac{1}{N} \sum_{n=1}^N \mathbb{E}_{q_\phi(z|x_n)} \left[(x_n^{(d)} - f_\theta(z)^{(d)})^2 \right] \quad (30)$$

□

C Experimental Details

Initialization at Global Optima of the VAE Objective The decoder function f_θ is initialized to the ground-truth using full supervision given the ground-truth z 's and $f_{\theta_{\text{GT}}}$. The encoder is initialized to ϕ_{GT} by fixing the decoder at the ground-truth and maximizing the ELBO (with the 10 random restarts). We fix the observation error σ_ϵ^2 to that of the ground truth model, and we fix a sufficiently flexible architecture – one that is significantly more expressive than needed to capture $f_{\theta_{\text{GT}}}$ – to ensure that, if there exists a f_θ with simpler posteriors, it would be included in our feasible set \mathcal{F} . Lastly, we select the restart that yields the lowest value of the objective function.

Synthetic Datasets We use 4 synthetic data-sets for unsupervised VAEs (described in Appendix F), and 2 synthetic data-sets for semi-supervised VAEs (described in Appendix G), and generate 5 versions of each data-set (each with 5000/2000/2000 train/validation/test points). We use 3 real semi-supervised data-sets: Diabetic Retinopathy Debrecen [3], Contraceptive Method Choice [1, 11] and the Titanic [1, 47] datasets, each with 10% observed labels, split in 5 different ways equally into train/validation/test.

Real Datasets We consider 3 UCI data-sets: Diabetic Retinopathy Debrecen [3], Contraceptive Method Choice [1, 11] and the Titanic [1, 47] datasets. In these, we treat the outcome as a partially observed label (observed 10% of the time). We split the data 5 different ways into equally sized train/validation/test. On each split of the data, we run 5 random restarts and select the run that yielded the best value on the training objective, computed on the validation set.

Evaluation Metrics To evaluate the quality of the generative model, we use the smooth k NN test statistic [10] on samples from the learned model vs. samples from the training set / ground truth model as an alternative to log-likelihood, since log-likelihood has been shown to be problematic for evaluation because of its numerical instability / high variance [48, 53]. In the semi-supervised case, we also use the smooth k NN test statistic to compare $p(x|y)$ with the learned $p_\theta(x|y)$. Finally, in cases where we may have model mismatch, we also evaluate the mutual information between x and each dimension of the latent space z , using the estimator presented in [29].

Architectures On the synthetic data-sets, we use a leaky-ReLU encoder/decoder with 3 hidden layers, each 50 nodes. On the UCI data-sets, we use a leaky-ReLU encoder/decoder with 3 hidden layers, each 100 nodes.

Optimization For optimization, we use the Adam optimizer [22] with a learning rate of 0.001 and a mini-batch size of 100. We train for 100 epochs on synthetic data and for 20000 on real data (and verified convergence). We trained 5 random restarts on each of the split of the data. For semi-supervised data-sets with discrete labels, we used continuous relaxations of the categorical distribution with temperature 2.2 [18] as the variational family in order to use the reparameterization trick [26].

Baselines For our baselines, we compare the performance of a MFG-VAE with that of a VAE trained with the Lagging Inference Networks (LIN) algorithm (still with a MFG variational family), since the algorithm claims to be able to escape local optima in training. Since the pathologies we describe are global optima, we do not expect LIN to mitigate the issues. We use Importance Weighted Autoencoders (IWAE) as an example of a inference algorithm that uses a more complex variational family. Since the pathologies described are exacerbated by a limited variational family, we expect IWAE to out-perform the other two approaches. For each method, we select the hyper-parameters for which the best restart yields the best log-likelihood (using the smooth k NN test-statistic, described below).

Hyper-parameters When using IWAE, let S be the number of importance samples used. When using the Lagging Inference Networks, let T be the threshold for determining whether the inference network objective has converged, and let R be the number of training iterations for which the loss is averaged before comparing with the threshold. When using semi-supervision, α determines the weight of the discriminator, and γ determines the weight of the labeled objective, \mathcal{L} . We grid-searched over all combination of the following sets of parameters:

Unsupervised datasets:

- IWAE: $S \in \{3, 10, 20\}$
- Lagging Inference Networks: $T \in \{0.05, 0.1\}$, $R \in \{5, 10\}$

Semi-supervised synthetic datasets:

- IWAE: $S \in \{3, 10, 20\}$
- Lagging Inference Networks: $T \in \{0.05, 0.1\}$, $R \in \{5, 10\}$
- All methods: $\alpha \in \{0.0, 0.1, 1.0\}$, $\gamma \in \{0.5, 1.0, 2.0, 5.0\}$

Semi-supervised real datasets:

- IWAE: $S \in \{3, 10, 20\}$
- Lagging Inference Networks: $T \in \{0.05, 0.1\}$, $R \in \{5, 10\}$
- All methods: $\alpha \in \{0.0, 0.1, 1.0\}$, $\gamma \in \{0.5, 1.0, 2.0, 5.0\}$, $\sigma_\epsilon^2 \in \{0.01, 0.5\}$. On Titanic dimensionality of z is $\in \{1, 2\}$, on Contraceptive and Diabetic Retinopathy $\in \{2, 5\}$.

Hyper-parameters Selection For each method, we selected the hyper-parameters that yielded the smallest value of the smooth k NN test statistic (indicating that they learned the $p(x)$ best).

D Quantitative Results

In this section we present the quantitative results for the paper. For all data-sets, we fix a sufficiently flexible architecture (one that is significantly more expressive than needed to capture $f_{\theta_{\text{GT}}}$) so that our feasible set \mathcal{F} is diverse enough to include likelihoods with simpler posteriors. For the synthetic data-sets, we then train each model to reach the global optima as follows: we train 10 restarts for each method and hyper-parameter settings – 5 random where we initialize randomly, and 5 random where the decoder and encoder are initialized to ground truth values. We select the restart with the best value of the objective function. See Appendix C for a complete detail on the experimental setup.

D.1 Approximation of $p(x)$ is poor when both conditions of Theorem 1 hold

Here we show that on data-sets for which Theorem 1 holds, VAEs approximate $p(x)$ poorly. We do this on two data-sets, the “Figure-8” and the “Clusters” Examples (described in Appendices F.1 and F.4, respectively). Table 1 shows that these data-sets, VAEs (even with a better training algorithm, LIN) approximate $p(x)$ poorly, while methods with a more complex variational family (like IWAE) do not. Visualization of the posterior (in Appendix H.1) confirm that the VAE objective under-fits the generative model in order to learn a simpler posterior, whereas the IWAE objective does not: for the “Figure-8 Example” see Figures 6, 7 and 8, and for the “Clusters Example” see Figures 9, 10 and 11. In these two examples, we further see the ELBO’s regularizing effect on the learned f_θ . On the “Figure-8 Example”, the learned f_θ ensures that x ’s generated from $z \in [-\infty, -3] \cup [3, \infty]$ are sufficiently different from x ’s generated from $z \approx 0$: $f_\theta(z)$ curls away from the center $z \approx 0$ and thus simplifies the posterior. On the “Clusters Examples”, the learned f_θ has less pronounced changes in slope, and thus a simpler posterior.

D.2 Failure to Learn Disentangled Representations due to Theorem 1

In disentangled representation learning, we suppose that each dimension of the latent space corresponds to a task-meaningful concept [40, 5]. Our goal is to infer these meaningful ground truth latent dimensions. It’s been noted in literature that this inference problem is ill-posed - that is, there are an infinite number of likelihood functions (and hence latent codes) that can capture $p(x)$ equally well [30]. Here, we show that, more problematically, the VAE objective can *prefer* learning the representations that *entangles* the ground-truth latent dimensions due to the pathology in Theorem 1.

Consider data generated by $f_{\theta_{\text{GT}}}(z) = Az + b$. If A is non-diagonal, then the posteriors of this model are correlated Gaussians (poorly approximated by MFGs). Let $A' = AR$, where we define $R = (\Sigma V^\top)^{-1}(\Lambda - \sigma_\epsilon^2 I)^{1/2}$ with an arbitrary diagonal matrix Λ and matrices Σ, V taken from the SVD of A , $A = U\Sigma V^\top$. In this case, $f_\theta = A'z + b$ has the same marginal likelihood as $f_{\theta_{\text{GT}}}$, that is, $p_\theta(x) = p_{\theta_{\text{GT}}}(x) = \mathcal{N}(b, \sigma_\epsilon^2 \cdot I + AA^\top)$. However, since the posteriors of f_θ are uncorrelated, the ELBO will prefer f_θ over $f_{\theta_{\text{GT}}}$! In the latent space corresponding to f_θ , the original *interpretations* of the latent dimensions are now entangled.

Similarly, for more complicated likelihood functions, we expect the ELBO to prefer learning models with simpler posteriors which are not necessarily ones that are useful for constructing disentangled representations. This bias is reduced in the IWAE training objective.

D.3 VAE training pathologies hinder learning compressed representations due to Theorem 1

In practice, if the task does not require a specific latent space dimensionality, K , one chooses K that maximizes the $\log p_\theta(x)$. Note that using a higher K and a lower σ_ϵ^2 means we can capture the data distribution with a simpler function $f_\theta(z)$ and hence get simpler posteriors. That is, increasing K alleviates the need to compromise the generative model in order to improve the inference model and leads to better approximation of $p(x)$. Thus, the ELBO will favor model mismatch (K larger than the ground truth) and prevent us from learning highly compressed representations when they are available.

We demonstrate this empirically by embedding the “Figure-8” and “Clusters” Examples into a 5D space using a linear transformation, $A = \begin{pmatrix} 1.0 & 0.0 & 0.5 & 0.2 & -0.8 \\ 0.0 & 1.0 & -0.5 & 0.3 & -0.1 \end{pmatrix}$, and then training a VAE with latent dimensionality $K \in \{1, 2, 3\}$, with $K = 1$ corresponding to the ground-truth model. Training for $K = 1$ is initialized at the ground truth model, and for $K > 2$ we initialize randomly; in each case we optimize σ_ϵ^2 per-dimension to minimize the negative ELBO. The ELBO prefers models with larger K over the ground truth model ($K = 1$), and that as K increases, the average informativeness of each latent code decreases (Table 2), since the latent space learns to generate the observation noise ϵ . We confirm that the posteriors become simpler as K increases, lessening the incentive for the VAE to compromise on approximating $p(x)$ (Figure 20). Lastly, we confirm that while LIN also shows preference for higher K ’s, IWAE does not (Table 2).

D.4 VAEs trade-off between generating realistic data and realistic counterfactuals in semi-supervision due to Theorem 1

Trade-offs when labels are discrete The trade-off between realistic data and realistic counterfactuals generation is demonstrated in the “Discrete Semi-Circle” Example, visualized in Figure 13 (details in Appendix G.1). The VAE is able to learn the data manifold and distribution well (Figure 13a). However, the learned model has a simple posterior in comparison to the true posterior (Figure 13f). In fact, the learned $f_\theta(z, y)$ is collapsed to the same function for all values of y (Figure 13b). As a result, $p_\theta(x|y) \approx p_\theta(x)$ under the learned model (Figure 13c). We call this phenomenon “functional collapse”. As expected, functional collapse occurs when training with LIN as well (Figure 14). In contrast, IWAE is able to learn two distinct data conditionals $p_\theta(x|y)$, but it does so at a cost. ***Since IWAE does not regularize the generative model, it overfits*** (Figure 15). Table 3 shows that IWAE learns $p(x)$ worse than the VAE, while Table 4 shows that it learns $p(x|y)$ significantly better. We see a similar pattern in the real data-sets (see Tables 5 and 6).

Trade-offs when labels are continuous When y is discrete, we can lower-bound the number of modes of $p_\theta(z|x)$ by the number of distinct values of y , and choose a variational family that is sufficiently expressive. But when y is continuous, we cannot easily bound the complexity of $p_\theta(z|x)$. In this case, we show that the same trade-off between realistic data and realistic counterfactuals exists, and that there is an *additional* pathology introduced by the discriminator $q_\phi(y|x)$ (Equation 9). Consider the “Continuous Semi-Circle” Example, visualized in Figure 16b (details in Appendix G.2). Here, since the posterior $p_\theta(y|x)$ is bimodal, encouraging the MFG discriminator $q_\phi(y|x)$ to be predictive will collapse $f_\theta(y, z)$ to the same function for all y (Figure 16b). So as we increase α (the priority placed on prediction), our predictive accuracy increases at the cost of collapsing $p_\theta(x|y)$ towards $p_\theta(x)$. The latter will result in low quality counterfactuals (see Figure 16c). Like in the discrete case, γ still controls the tradeoff between realistic data and realistic counterfactuals; in the continuous case, α *additionally* controls the tradeoff between realistic counterfactuals and predictive accuracy. Table 4 shows that IWAE is able to learn $p(x)$ better than VAE and LIN, as expected, but ***the naive addition of the discriminator to IWAE means that it learns $p(x|y)$ no better than the other two models*** (see below for an explanation); that is, with the naive discriminator, just like the VAE and LIN, IWAE suffers from functional collapse (see Figure 18).

Naive application adaptation of IWAE for semi-supervision introduces new pathologies. The variational family implied by the IWAE objective is not the one given by the IWAE decoder q_ϕ [7]. As such, incorporating a discriminator term $q_\phi(y|x)$ into an IWAE semi-supervised objective is non-trivial, since the real approximate variational family used is complex and requires intractable marginalization over z . Although some get around this intractability by working with lower bounds [45] on $q_\phi(y, z|x)$ marginalized over z , the discriminator in these cases is nonetheless different from the variational posterior. This may be an additional factor of the poor performance of IWAE in the semi-supervised setting with continuous y .

Data	IWAE	LIN	VAE
Clusters	0.057 ± 0.028	0.347 ± 0.057	0.361 ± 0.083
Fig-8	0.036 ± 0.013	0.040 ± 0.081	0.066 ± 0.014

Table 1: Comparison unsupervised learned vs. true data distributions via the smooth k NN test (lower is better). Hyper-parameters selected via smaller value of the loss function on the validation set.

VAE	Figure-8 Example			Clusters Example		
	$K = 1$ (ground-truth)	$K = 2$	$K = 3$	$K = 1$ (ground-truth)	$K = 2$	$K = 3$
Test - ELBO	-0.127 ± 0.057	-0.260 ± 0.040	-0.234 ± 0.050	4.433 ± 0.049	4.385 ± 0.034	4.377 ± 0.024
Test $\text{avg}_i I(x; z_i)$	2.419 ± 0.027	1.816 ± 0.037	1.296 ± 0.064	1.530 ± 0.011	1.425 ± 0.019	1.077 ± 0.105

IWAE	Figure-8 Example			Clusters Example		
	$K = 1$ (ground-truth)	$K = 2$	$K = 3$	$K = 1$ (ground-truth)	$K = 2$	$K = 3$
Test - ELBO	-0.388 ± 0.044	-0.364 ± 0.051	-0.351 ± 0.045	4.287 ± 0.047	4.298 ± 0.054	4.295 ± 0.049
Test $\text{avg}_i I(x; z_i)$	2.159 ± 0.088	1.910 ± 0.035	1.605 ± 0.087	1.269 ± 0.052	1.321 ± 0.033	1.135 ± 0.110

Table 2: The ELBO prefers learning models with more latent dimensions (and smaller σ_ϵ^2) over the ground truth model ($k = 1$). Although the models preferred by the ELBO have a higher mutual information between the data and learned z 's, the mutual information between dimension of z and the data decreases since with more latent dimensions, the latent space learns ϵ . In contrast, IWAE does not suffer from this pathology. LIN was not included here because it was not able to minimize the negative ELBO as well as the VAE on these data-sets.

Data	IWAE	LIN	VAE
Discrete Semi-Circle	0.694 ± 0.096	0.703 ± 0.315	0.196 ± 0.078
Continuous Semi-Circle	0.015 ± 0.011	0.128 ± 0.094	0.024 ± 0.014

Table 3: Comparison of semi-supervised learned vs. true data distributions via the smooth k NN test (lower is better). Hyper-parameters selected via the smooth k NN test-statistic computed on the data marginals.

Data	IWAE		LIN		VAE	
	Cohort 1	Cohort 2	Cohort 1	Cohort 2	Cohort 1	Cohort 2
Discrete Semi-Circle	1.426 ± 1.261	1.698 ± 0.636	18.420 ± 1.220	10.118 ± 0.996	15.206 ± 1.200	11.501 ± 1.300
Continuous Semi-Circle	15.951 ± 3.566	14.416 ± 1.402	15.321 ± 1.507	17.530 ± 1.509	13.128 ± 0.825	16.046 ± 1.019

Table 4: Comparison of semi-supervised learned $p_\theta(x|y)$ with ground truth $p(x|y)$ via the smooth k NN test statistic (smaller is better). Hyper-parameters selected via smallest smooth k NN test statistic computed on the data marginals. For the discrete data, the cohorts are $p(x|y = 0)$ and $p(x|y = 1)$, and for the continuous data, the cohorts are $p(x|y = -3.5)$ and $p(x|y = 3.5)$.

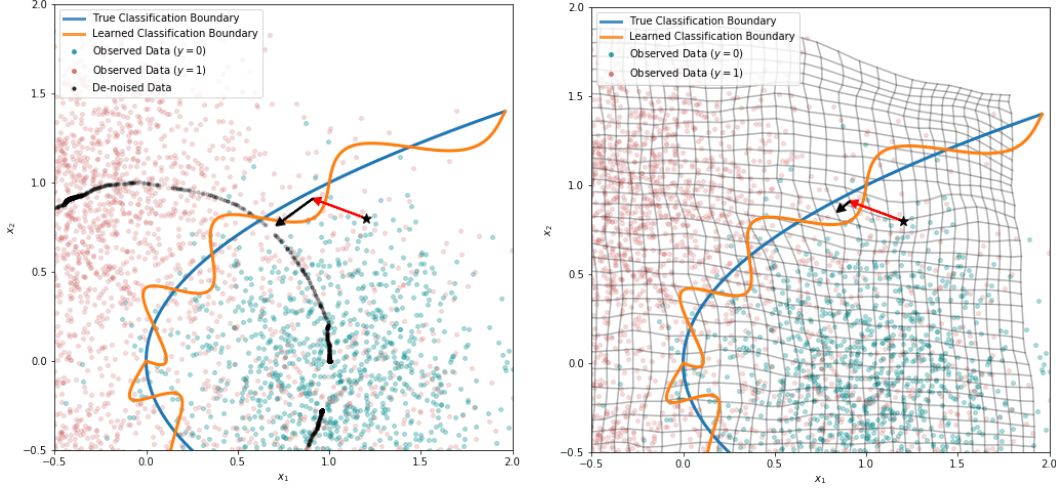
	IWAE	VAE
Diabetic Retinopathy	3.571 ± 2.543	6.206 ± 1.035
Contraceptive	1.740 ± 0.290	2.147 ± 0.225
Titanic	2.794 ± 1.280	1.758 ± 0.193

Table 5: Comparison of semi-supervised learned vs. true data distributions via the smooth k NN test (lower is better). Hyper-parameters selected via the smooth k NN test-statistic computed on the data marginals.

	IWAE			VAE		
	Cohort 1	Cohort 2	Cohort 3	Cohort 1	Cohort 2	Cohort 3
Diabetic Retinopathy	4.240 ± 1.219	4.357 ± 3.417	N/A	5.601 ± 0.843	8.008 ± 1.096	N/A
Contraceptive	7.838 ± 1.138	5.521 ± 3.519	6.626 ± 2.571	5.388 ± 0.788	4.994 ± 0.932	3.722 ± 0.488
Titanic	3.416 ± 0.965	6.923 ± 1.924	N/A	3.730 ± 0.866	8.572 ± 1.766	N/A

Table 6: Comparison of semi-supervised learned vs. true conditional distributions $p(x|y)$ via the smooth k NN test (lower is better). Hyper-parameters selected via the smooth k NN test-statistic computed on the data marginals.

E Defense Against Adversarial Perturbations Requires the True Observation Noise and Latent Dimensionality



(a) Projection of adversarial example onto true manifold.

(b) Projection of adversarial example onto manifold learned given model mismatch (higher dimensional latent space and smaller observation noise).

Figure 3: Comparison of projection of adversarial example onto ground truth vs. learned manifold. The star represents the original point, perturbed by the red arrow, and then projected onto the manifold by the black arrow.

As a defense against adversarial attacks, manifold-based approaches de-noise the data before feeding to a classifier with the hope that the de-noising will remove the adversarial perturbation from the data [17, 34, 43, 16, 19]. In this section we argue that a correct decomposition of the data into $f_\theta(z)$ and ϵ (or “signal” and “noise”) is necessary to prevent against certain perturbation-based adversarial attacks.

Assume that our data was generated as follows:

$$\begin{aligned} z &\sim p(z) \\ \epsilon &\sim \mathcal{N}(0, \sigma_\epsilon^2 \cdot I) \\ x|z &\sim f_{\theta_{\text{GT}}}(z) + \epsilon \\ y|z &\sim \text{Cat}(g_\psi \circ f_{\theta_{\text{GT}}}(z)) \end{aligned} \tag{31}$$

Let $\mu_\phi(x)$ denote the mean of encoder and let $M_{\theta,\phi}(x) = f_\theta \circ \mu_\phi(x)$ denote a projection onto the manifold. Our goal is to prevent adversarial attacks on a given discriminative classifier that predicts $y|x$ – that is, we want to ensure that there does not exist any η such that $x_n + \eta$ is classified with a different label than y_n by the learned classifier and not by the ground truth classifier. Since the labels y are computed as a function of the de-noised data, $f_{\theta_{\text{GT}}}(z)$, the true classifier is only defined on the manifold M (marked in blue in Figure 3). As such, any learned classifier (in orange) will intersect the true classifier on M , but may otherwise diverge from it away from the manifold. This presents a vulnerability against adversarial perturbations, since now any x can be perturbed to cross the learned classifier’s boundary (in orange) to flip its label, while its true label remains the same, as determined by the true classifier (in blue). To protect against this vulnerability, existing methods de-noise the data by projecting it onto the manifold before classifying. Since the true and learned classifiers intersect on the manifold, in order to flip an x ’s label, the x must be perturbed to cross the true classifier’s boundary (and not just the learned classifier’s boundary). This is illustrated in Figure 3a: the black star represents some data point, perturbed (by the red arrow) by an adversary to cross the learned classifier’s boundary but not the true classifier’s boundary. When projected onto the manifold (by the black arrow), the adversarial attack still falls on the same side of the true classifier and the learned classifier, rendering the attack unsuccessful and this method successful.

However, if the manifold is not estimated correctly from the data (i.e. if the ground truth dimensionality of the latent space and the observation noise σ_ϵ^2 are poorly estimated), this defense may fail. Consider, for example, the case in which $f_\theta(z)$ is modeled with a VAE with a larger dimensional latent space and a smaller observation noise than the ground truth model. Figure 3b shows a uniform grid in x 's space projected onto the manifold learned by this mismatched model. The figure shows that the learned manifold barely differs from the original space, since the latent space of the VAE compensates for the observation noise ϵ and thus does not de-noise the observation. When the adversarial attack is projected onto the manifold, it barely moves and is thus left as noisy. As the figure shows, the attack crosses the learned classifier's boundary but not the true boundary and is therefore successful.

F Unsupervised Pedagogical Examples

In this section we describe in detail the unsupervised pedagogical examples used in the paper and the properties that cause them to trigger the VAE pathologies. For each one of these example decoder functions, we fit a surrogate neural network f_θ using full supervision (ensuring that the $\text{MSE} < 1e-4$ and use that f_θ to generate the actual data used in the experiments.

F.1 Figure-8 Example

Generative Process:

$$\begin{aligned} z &\sim \mathcal{N}(0, 1) \\ \epsilon &\sim \mathcal{N}(0, \sigma_\epsilon^2 \cdot I) \\ u(z) &= (0.6 + 1.8 \cdot \Phi(z)) \pi \\ x|z &= \underbrace{\begin{bmatrix} \frac{\sqrt{2}}{2} \cdot \frac{\cos(u(z))}{\sin(u(z))^2 + 1} \\ \sqrt{2} \cdot \frac{\cos(u(z)) \sin(u(z))}{\sin(u(z))^2 + 1} \end{bmatrix}}_{f_{\theta_{\text{GT}}}(z)} + \epsilon \end{aligned} \quad (32)$$

where $\Phi(z)$ is the Gaussian CDF and $\sigma_\epsilon^2 = 0.02$ (see Figure 6).

Properties: In this example, values of z on $[-\infty, -3.0]$, $[3.0, \infty]$ and in small neighborhoods of $z = 0$ all produce similar values of x , namely $x \approx 0$; as such, the true posterior $p_{\theta_{\text{GT}}}(z|x)$ is multi-modal in the neighborhood of $x = 0$ (see Figure 6d), leading to high PMO. Additionally, in the neighborhood of $x \approx 0$, $p(x)$ is high. Thus, condition (1) of Theorem 1 is satisfied. One can verify condition (2) is satisfied by considering all continuous parametrizations of a figure-8 curve. Any such parametrization will result in a f_θ for which far-away values of z lead to nearby values of x and thus in high PMO value for points near $x = 0$.

F.2 Circle Example

Generative Process:

$$\begin{aligned} z &\sim \mathcal{N}(0, 1) \\ \epsilon &\sim \mathcal{N}(0, \sigma_\epsilon^2 \cdot I) \\ x|z &= \underbrace{\begin{bmatrix} \cos(2\pi \cdot \Phi(z)) \\ \sin(2\pi \cdot \Phi(z)) \end{bmatrix}}_{f_{\theta_{\text{GT}}}(z)} + \epsilon \end{aligned} \quad (33)$$

where $\Phi(z)$ is the Gaussian CDF and $\sigma_\epsilon^2 = 0.01$ (see Figure 4).

Properties: In this example, the regions of the data-space that have a non-Gaussian posterior are near $x \approx [1.0, 0.0]$, since in that neighborhood, $z \in [-\infty, -3.0]$ and $z \in [3.0, \infty]$ both generate nearby values of x . Thus, this model only satisfies condition 2 of Theorem 1. However, since overall the number of x 's for which the posterior is non-Gaussian are few, the VAE objective does not need to trade-off capturing $p(x)$ for easy posterior approximation. We see that traditional training is capable of recovering $p(x)$, regardless of whether training was initialized randomly or at the ground truth (see Figure 4).

F.3 Absolute-Value Example

Generative Process:

$$\begin{aligned} z &\sim \mathcal{N}(0, 1) \\ \epsilon &\sim \mathcal{N}(0, \sigma_\epsilon^2 \cdot I) \\ x|z &= \underbrace{\begin{bmatrix} \Phi(z) \\ |\Phi(z)| \end{bmatrix}}_{f_{\theta_{\text{GT}}}(z)} + \epsilon \end{aligned} \quad (34)$$

where $\Phi(z)$ is the Gaussian CDF and $\sigma_\epsilon^2 = 0.01$ (see Figure 5).

Properties: In this example, the posterior under $f_{\theta_{\text{GT}}}$ cannot be well approximated using a MFG variational family (see Figure 5d). However, there does exist an alternative likelihood function $f_\theta(z)$ (see 5b) that explains $p(x)$ equally well and has simpler posterior 5e. As such, this model only satisfies condition 1 of Theorem 1.

F.4 Clusters Example

Generative Process:

$$\begin{aligned} z &\sim \mathcal{N}(0, 1) \\ \epsilon &\sim \mathcal{N}(0, \sigma_\epsilon^2 \cdot I) \\ u(z) &= \frac{2\pi}{1 + e^{-\frac{1}{2}\pi z}} \\ t(u) &= 2 \cdot \tanh(10 \cdot u - 20 \cdot \lfloor u/2 \rfloor - 10) + 4 \cdot \lfloor u/2 \rfloor + 2 \\ x|z &= \underbrace{\begin{bmatrix} \cos(t(u(z))) \\ \sin(t(u(z))) \end{bmatrix}}_{f_{\theta_{\text{GT}}}(z)} + \epsilon \end{aligned} \quad (35)$$

where $\sigma_\epsilon^2 = 0.2$.

Properties: In this example, $f_{\theta_{\text{GT}}}$ a step function embedded on a circle. Regions in which $\frac{df_{\theta_{\text{GT}}}^{-1}}{dx}$ is high (i.e. the steps) correspond to regions in which $p(x)$ is high. The interleaving of high density and low density regions on the manifold yield a multi-modal posterior (see Figure 9d). For this model, both conditions of Theorem 1 hold. In this example, we again see that the VAE objective learns a model with a simpler posterior (see Figure 9e) at the cost of approximating $p(x)$ well (see Figure 9a).

F.5 Spiral Dots Example

Generative Model:

$$\begin{aligned} z &\sim \mathcal{N}(0, 1) \\ \epsilon &\sim \mathcal{N}(0, \sigma_\epsilon^2 \cdot I) \\ u(z) &= \frac{4\pi}{1 + e^{-\frac{1}{2}\pi z}} \\ t(u) &= \tanh(10 \cdot u - 20 \cdot \lfloor u/2 \rfloor - 10) + 2 \cdot \lfloor u/2 \rfloor + 1 \\ x|z &= \underbrace{\begin{bmatrix} t(u(z)) \cdot \cos(t(u(z))) \\ t(u(z)) \cdot \sin(t(u(z))) \end{bmatrix}}_{f_{\theta_{\text{GT}}}(z)} + \epsilon \end{aligned} \quad (36)$$

where $\sigma_\epsilon^2 = 0.01$.

Properties: In this example, $f_{\theta_{\text{GT}}}$ a step function embedded on a spiral. Regions in which $\frac{df_{\theta_{\text{GT}}}}{dx}$ is high (i.e. the steps) correspond to regions in which $p(x)$ is high. The interleaving of high density and low density regions on the manifold yield a multi-modal posterior (see Figure 12d). In this example, we again see that the VAE objective learns a model with a simpler posterior (see Figure 12e) at the cost of approximating $p(x)$ well (see Figure 12a). Furthermore, for this model the VAE objective highly misestimates the observation noise.

G Semi-Supervised Pedagogical Examples

In this section we describe in detail the semi-supervised pedagogical examples used in the paper and the properties that cause them to trigger the VAE pathologies. For each one of these example decoder functions, we fit a surrogate neural network f_{θ} using full supervision (ensuring that the $\text{MSE} < 1e - 4$ and use that f_{θ} to generate the actual data used in the experiments.

G.1 Discrete Semi-Circle Example

Generative Process:

$$\begin{aligned} z &\sim \mathcal{N}(0, 1) \\ y &\sim \text{Bern}\left(\frac{1}{2}\right) \\ \epsilon &\sim \mathcal{N}(0, \sigma_{\epsilon}^2 \cdot I) \\ x|y, z &= \underbrace{\begin{bmatrix} \cos\left(\mathbb{I}(y=0) \cdot \pi \cdot \sqrt{\Phi(z)} + \mathbb{I}(y=1) \cdot \pi \cdot \Phi(z)^3\right) \\ \sin\left(\mathbb{I}(y=0) \cdot \pi \cdot \sqrt{\Phi(z)} + \mathbb{I}(y=1) \cdot \pi \cdot \Phi(z)^3\right) \end{bmatrix}}_{f_{\theta_{\text{GT}}}(y, z)} + \epsilon \end{aligned} \quad (37)$$

where Φ is the CDF of a standard normal and $\sigma_{\epsilon}^2 = 0.01$.

Properties: We designed this data-set to specifically showcase issues with the semi-supervised VAE objective. As such, we made sure that the data marginal $p(x)$ of this example will be learned well using unsupervised VAE (trained on the x 's only) This way we can focus on the new issues introduced by the semi-supervised objective.

For this ground-truth model, the posterior of the un-labeled data $p_{\theta_{\text{GT}}}(z|x)$ is bimodal, since there are two functions that could have generated each x : $f_{\theta_{\text{GT}}}(y=0, z)$ and $f_{\theta_{\text{GT}}}(y=1, z)$. As such, approximating this posterior with a MFG will encourage the semi-supervised objective to find a model for which $f_{\theta_{\text{GT}}}(y=0, z) = f_{\theta_{\text{GT}}}(y=1, z)$ (see Figure 13b). When both functions collapse to the same function, $p_{\theta}(x|y) \approx p_{\theta}(x)$ (see Figure 13c). This will prevent the learned model from generating realistic counterfactuals.

G.2 Continuous Semi-Circle Example

Generative Process:

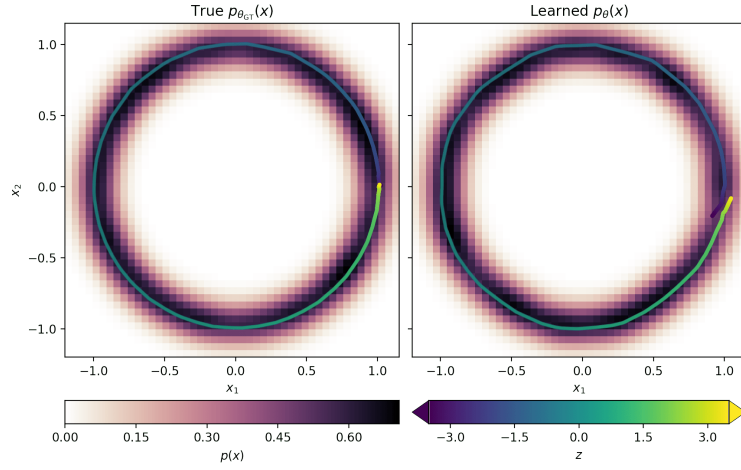
$$\begin{aligned} z &\sim \mathcal{N}(0, 1) \\ y &\sim \mathcal{N}(0, 1) \\ h(y) &= B^{-1}(\Phi(y); 0.2, 0.2) \\ \epsilon &\sim \mathcal{N}(0, \sigma_{\epsilon}^2 \cdot I) \\ x|y, z &= \underbrace{\begin{bmatrix} \cos\left(h(y) \cdot \pi \cdot \sqrt{\Phi(z)} + (1 - h(y)) \cdot \pi \cdot \Phi(z)^3\right) \\ \sin\left(h(y) \cdot \pi \cdot \sqrt{\Phi(z)} + (1 - h(y)) \cdot \pi \cdot \Phi(z)^3\right) \end{bmatrix}}_{f_{\theta_{\text{GT}}}(y, z)} + \epsilon \end{aligned} \quad (38)$$

where Φ is the CDF of a standard normal and $B^{-1}(\cdot; \alpha, \beta)$ is the inverse CDF of the beta distribution.

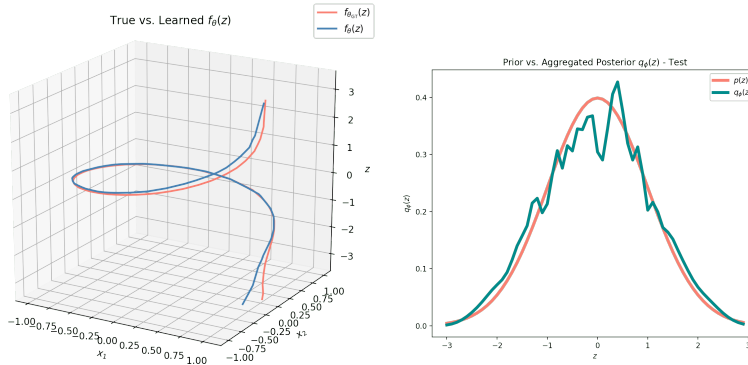
Properties: As in the “Discrete Semi-Circle Example”, we designed this data-set to have a $p(x)$ that the VAE objective would learn well so we can focus on the new issues introduced by the semi-supervised objective. The dataset demonstrates the same pathologies in the semi-supervised objective as shown by “Discrete Semi-Circle Example” with the addition of yet another pathology: since the posterior $p_\theta(y|x)$ is bimodal in this example, encouraging a MFG $q_\phi(y|x)$ discriminator to be predictive will collapse $f_\theta(y, z)$ to the same function for all values of y (see Figure 16b) As such, as we increase α , the better our predictive accuracy will be but the more $p_\theta(x|y) \rightarrow p_\theta(x)$, causing the learned model to generate poor quality counterfactuals (see Figure 16c).

H Qualitative Results

H.1 Qualitative results to support necessity of both conditions of Theorem 1

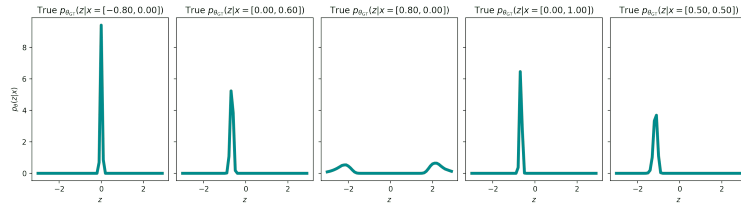


(a) True vs. learned $p_\theta(x)$, and learned vs. true $f_\theta(z)$, colored by the value of z .

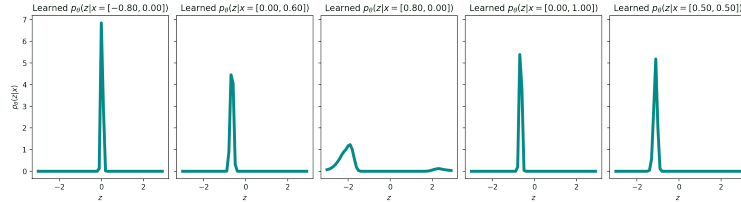


(b) True vs. learned $f_\theta(x)$

(c) Aggregated posterior vs. prior

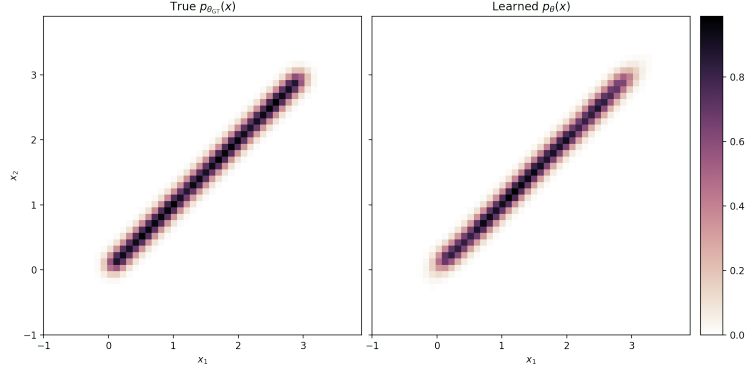


(d) Posters under true f_θ

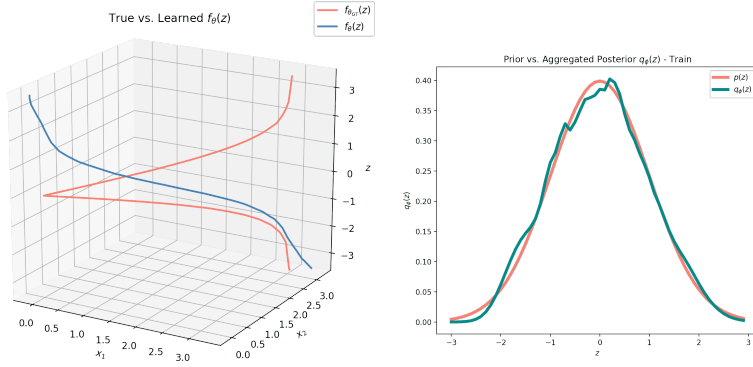


(e) Posteriors under learned f_θ

Figure 4: MFG-VAE trained on the Circle Example. In this toy data, condition (2) holds of Theorem 1 holds and condition (1) does not. To see this, notice that most examples of the posteriors are Gaussian-like, with the exception of the posteriors near $x = [1.0, 0.0]$, which are bimodal since in that neighborhood, x could have been generated using either $z > 3.0$ or using $z < -3.0$. Since only a few training points have a high posterior matching objective, a VAE is able to learn the data distribution well.

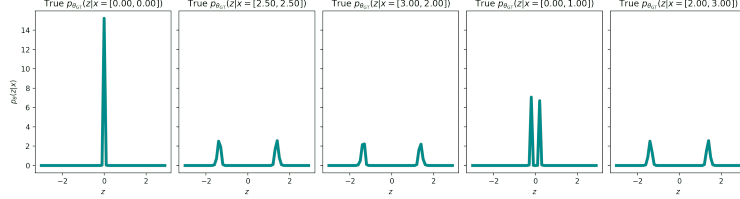


(a) True vs. learned $p_\theta(x)$

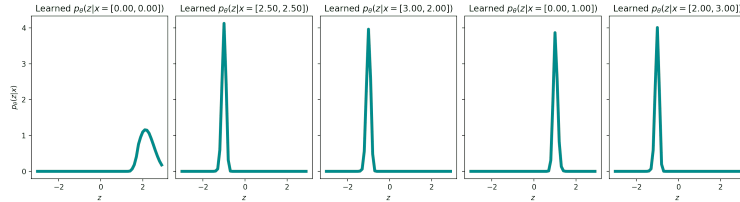


(b) True vs. learned $f_\theta(x)$

(c) Aggregated posterior vs. prior



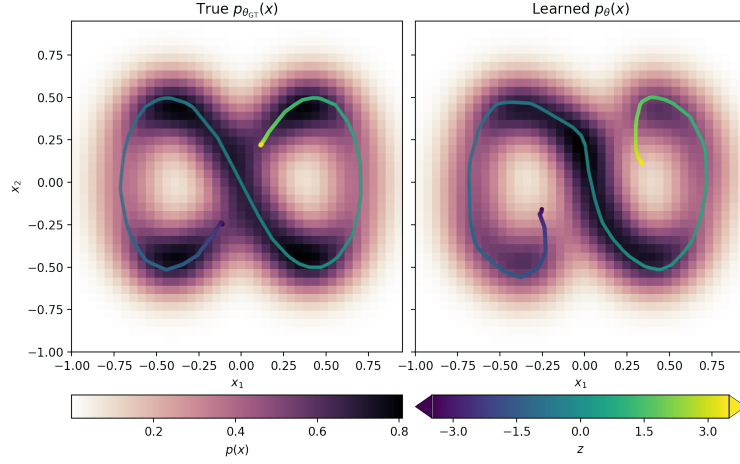
(d) Posteriors under true f_θ



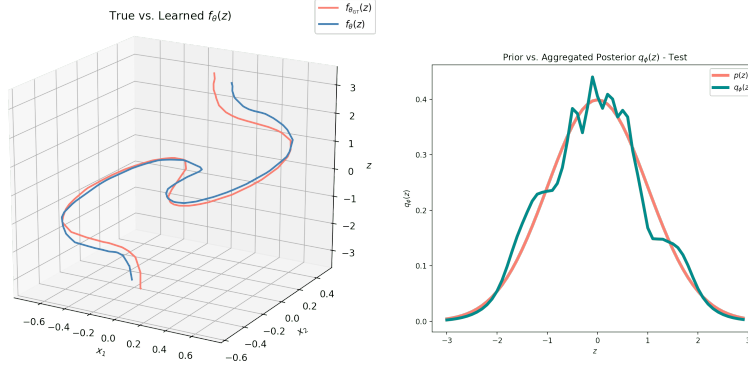
(e) Posteriors under learned f_θ

Figure 5: MFG-VAE trained on the Absolute-Value Example. In this toy data, condition (1) holds of Theorem 1 holds and condition (2) does not. To see this, notice that the function f_θ learned with a VAE is completely different than the ground-truth f_θ , and unlike the ground truth f_θ which has bimodal posteriors, the learned f_θ has unimodal posteriors (which are easier to approximate with a MFG). As such, a VAE is able to learn the data distribution well.

H.2 Qualitative Demonstration of Unsupervised VAE Pathologies

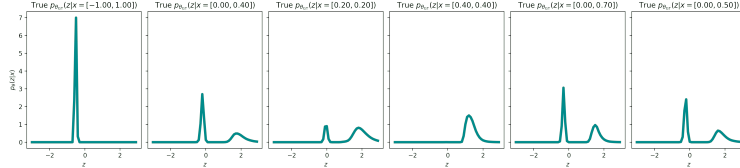


(a) True vs. learned $p_{\theta}(x)$, and learned vs. true $f_{\theta}(z)$, colored by the value of z .

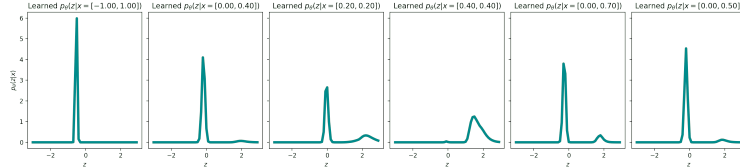


(b) True vs. learned $f_{\theta}(x)$

(c) Aggregated posterior vs. prior

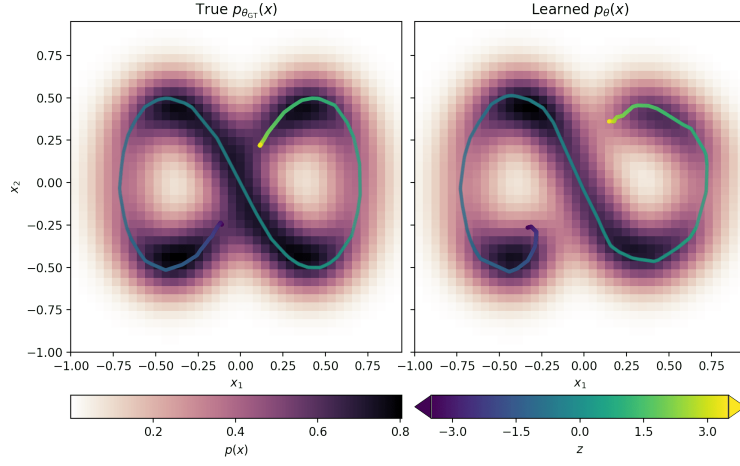


(d) Posteriors under true f_{θ}

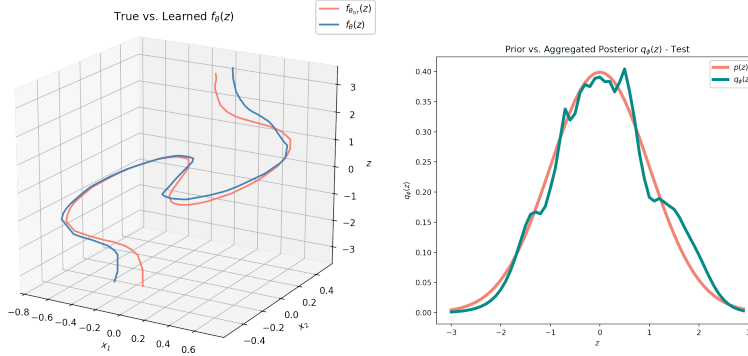


(e) Posteriors under learned f_{θ}

Figure 6: MFG-VAE trained on the Figure-8 Example. In this toy data, both conditions of Theorem 1 hold. The VAE learns a generative model with simpler posterior than that of the ground-truth, though it is unable to completely simplify the posterior as in the Absolute-Value Example. To learn a generative model with a simpler posterior, it curves the learned function f_{θ} at $z = -3.0$ and $z = 3.0$ away from the region where $z = 0$. This is because under the true generative model, the true posterior $p_{\theta}(z|x)$ in the neighborhood of $x \approx 0$ has modes around either $z = 0$ and $z = 3.0$, or around $z = 0$ and $z = -3.0$, leading to a high posterior matching objective.

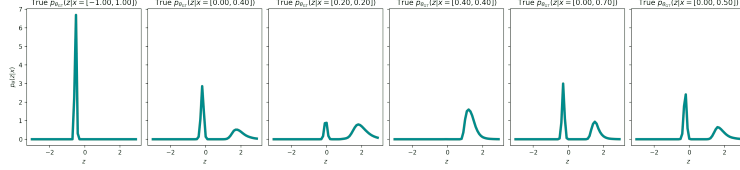


(a) True vs. learned $p_\theta(x)$, and learned vs. true $f_\theta(z)$, colored by the value of z .

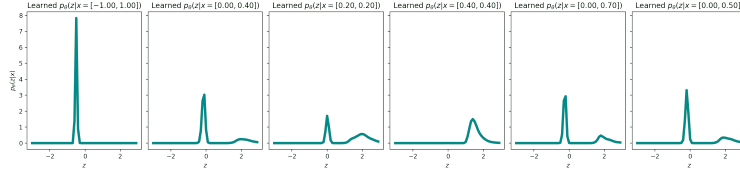


(b) True vs. learned $f_\theta(x)$

(c) Aggregated posterior vs. prior

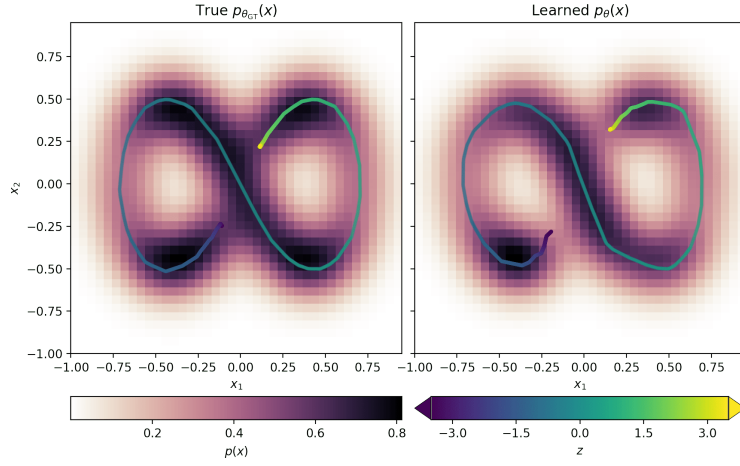


(d) Posteriors under true f_θ

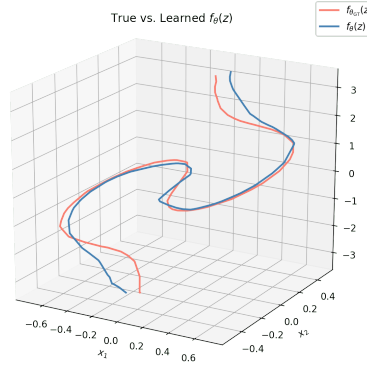


(e) Posteriors under learned f_θ

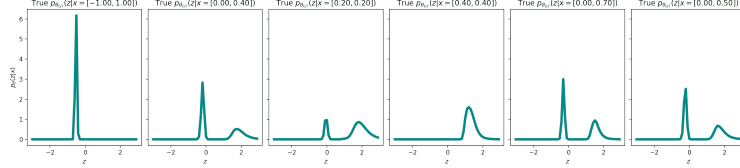
Figure 7: VAE with Lagging Inference Networks (LIN) trained on the Figure-8 Example. While LIN may help escape local optima, on this data, the training objective is still biased away from learning the true data distribution. As such, LIN fails in the same way a MFG-VAE does (see Figure 6).



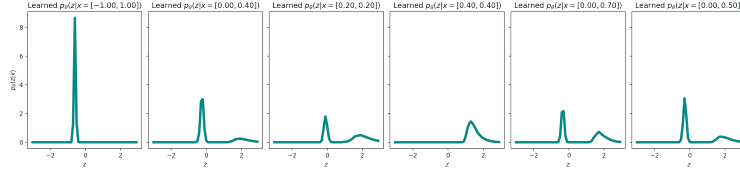
(a) True vs. learned $p_{\theta}(x)$, and learned vs. true $f_{\theta}(z)$, colored by the value of z .



(b) True vs. learned $f_{\theta}(x)$

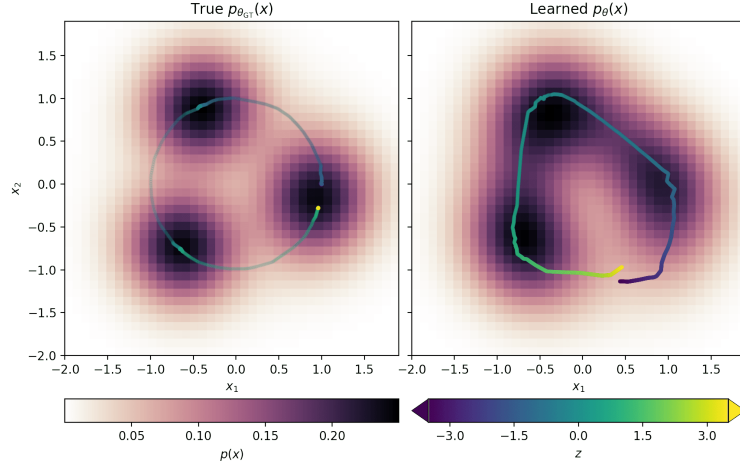


(c) Posteriors under true f_{θ}

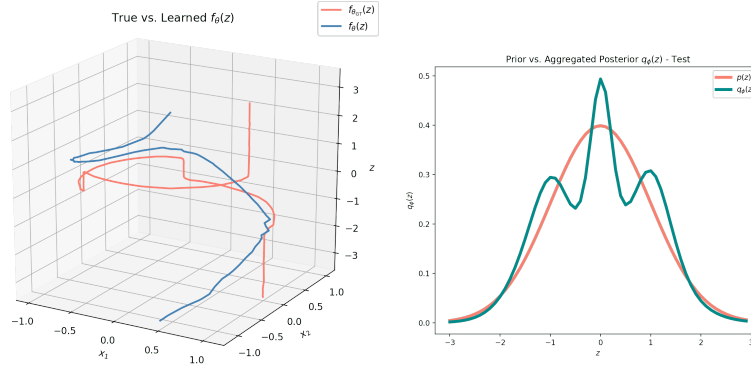


(d) Posteriors under learned f_{θ}

Figure 8: IWAE trained on the Figure-8 Example. In this toy data, both conditions of Theorem 1 hold. The IWAE learns a generative model with a slightly simpler posterior than that of the ground-truth. This is because even with the number of importance samples as large as $S = 20$, the variational family implied by the IWAE objective is not sufficiently expressive. The objective therefore prefers to learn a model with a lower data marginal likelihood. While increasing $S \rightarrow \infty$ will resolve this issue, it is not clear how large a S is necessary and whether the additional computational overhead is worth it.

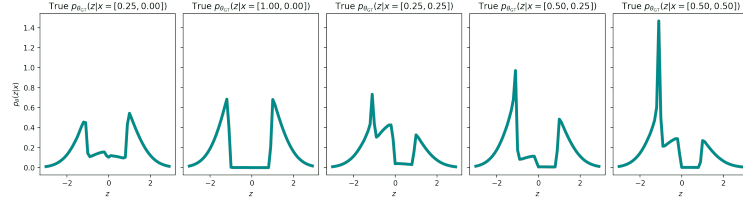


(a) True vs. learned $p_\theta(x)$, and learned vs. true $f_\theta(z)$, colored by the value of z .

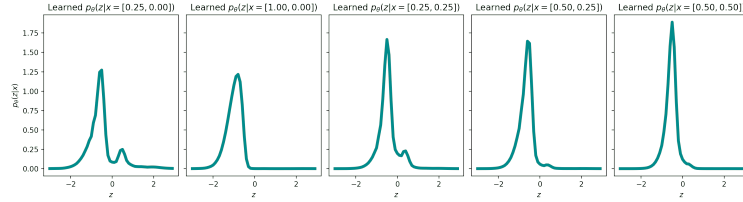


(b) True vs. learned $f_\theta(x)$

(c) Aggregated posterior vs. prior

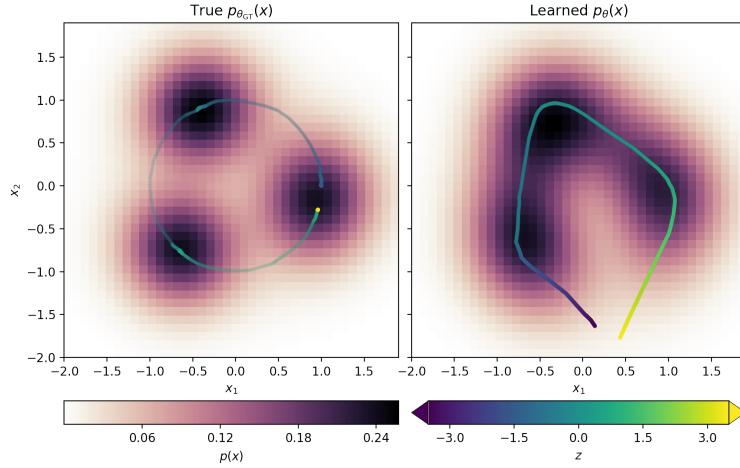


(d) Posters under true f_θ

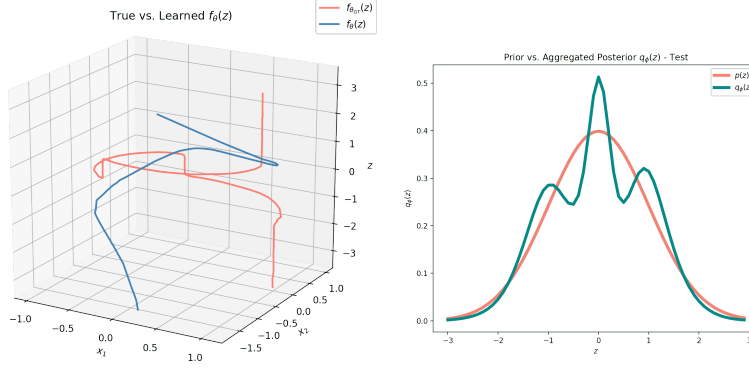


(e) Posters under learned f_θ

Figure 9: MFG-VAE trained on the Clusters Example. In this toy data, both conditions of Theorem 1 hold. The VAE learns a generative model with simpler posterior than that of the ground-truth, though it is unable to completely simplify the posterior as in the Absolute-Value Example. To learn a generative model with a simpler posterior, it learns a model with a function $f_\theta(z)$ that, unlike the ground truth function, does not have steep areas interleaved between flat areas. As such, the learned model is generally more flat, causing the learned density to be “smeared” between the modes.

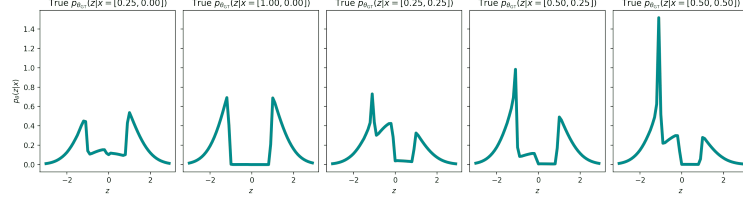


(a) True vs. learned $p_\theta(x)$, and learned vs. true $f_\theta(z)$, colored by the value of z .

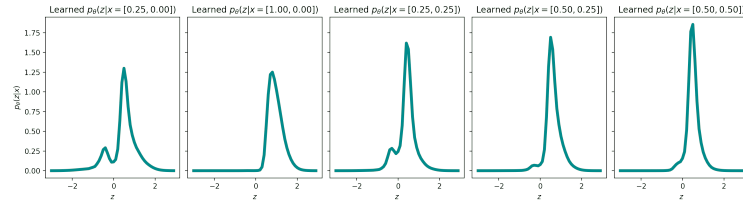


(b) True vs. learned $f_\theta(x)$

(c) Aggregated posterior vs. prior

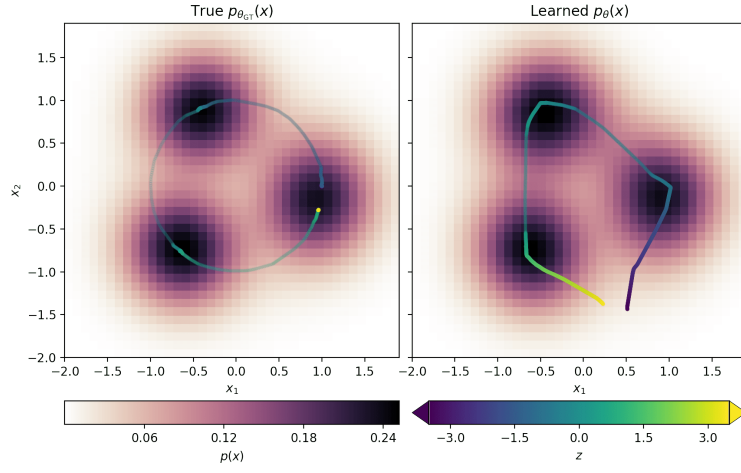


(d) Posteriors under true f_θ

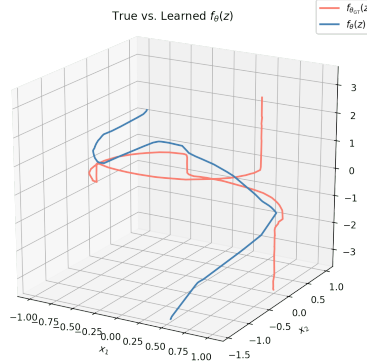


(e) Posteriors under learned f_θ

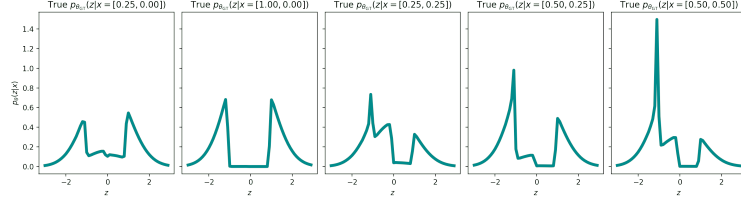
Figure 10: VAE with Lagging Inference Networks (LIN) trained on the Clusters Example. While LIN may help escape local optima, on this data, the training objective is still biased away from learning the true data distribution. As such, LIN fails in the same way a MFG-VAE does (see Figure 9).



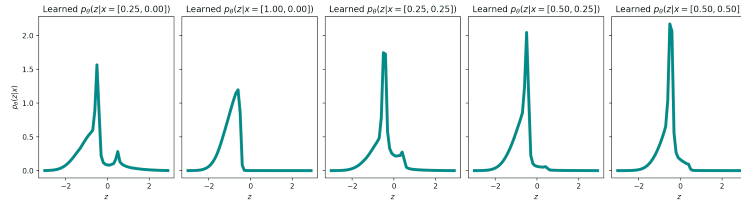
(a) True vs. learned $p_{\theta}(x)$, and learned vs. true $f_{\theta}(z)$, colored by the value of z .



(b) True vs. learned $f_{\theta}(x)$

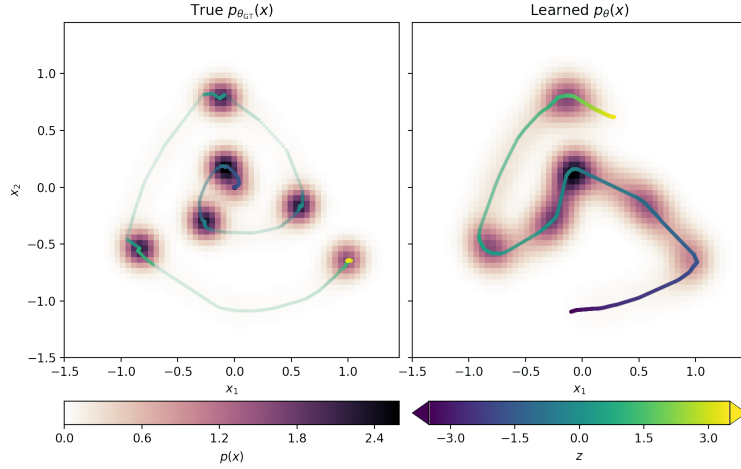


(c) Posteriors under true f_{θ}

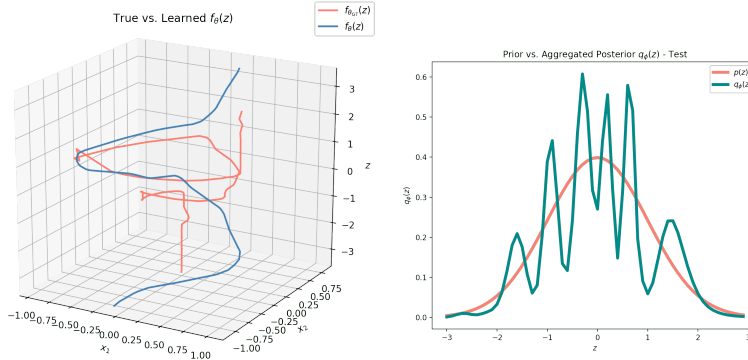


(d) Posteriors under learned f_{θ}

Figure 11: IWAE trained on the Clusters Example. In this toy data, both conditions of Theorem 1 hold. IWAE is able to learn the ground truth data distribution while finding a generative model with a simpler posterior than that of the ground-truth model.

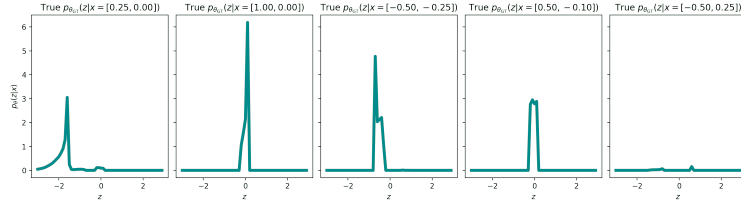


(a) True vs. learned $p_{\theta}(x)$, and learned vs. true $f_{\theta}(z)$, colored by the value of z .

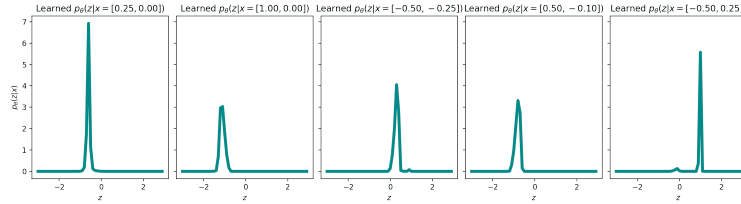


(b) True vs. learned $f_{\theta}(x)$

(c) Aggregated posterior vs. prior



(d) Posteriors under true f_{θ}



(e) Posteriors under learned f_{θ}

Figure 12: MFG-VAE trained on the Spiral-Dots Example jointly over $\theta, \phi, \epsilon_{\epsilon}^2$. In this toy data, as Theorem 2 predicts, the ELBO drastically misestimates the observation noise. The VAE learns a generative model with simpler posterior than that of the ground-truth, though it is unable to completely simplify the posterior as in the Absolute-Value Example. To learn a generative model with a simpler posterior, it learns a model with a function $f_{\theta}(z)$ that, unlike the ground truth function, does not have steep areas interleaved between flat areas. As such, the learned model is generally more flat, causing the learned density to be “smeared” between the modes. Moreover due to the error in approximating the true posterior with a MFG variational family, the ELBO misestimates σ_{ϵ}^2 .

H.3 Qualitative Demonstration of Semi-Supervised VAE Pathologies

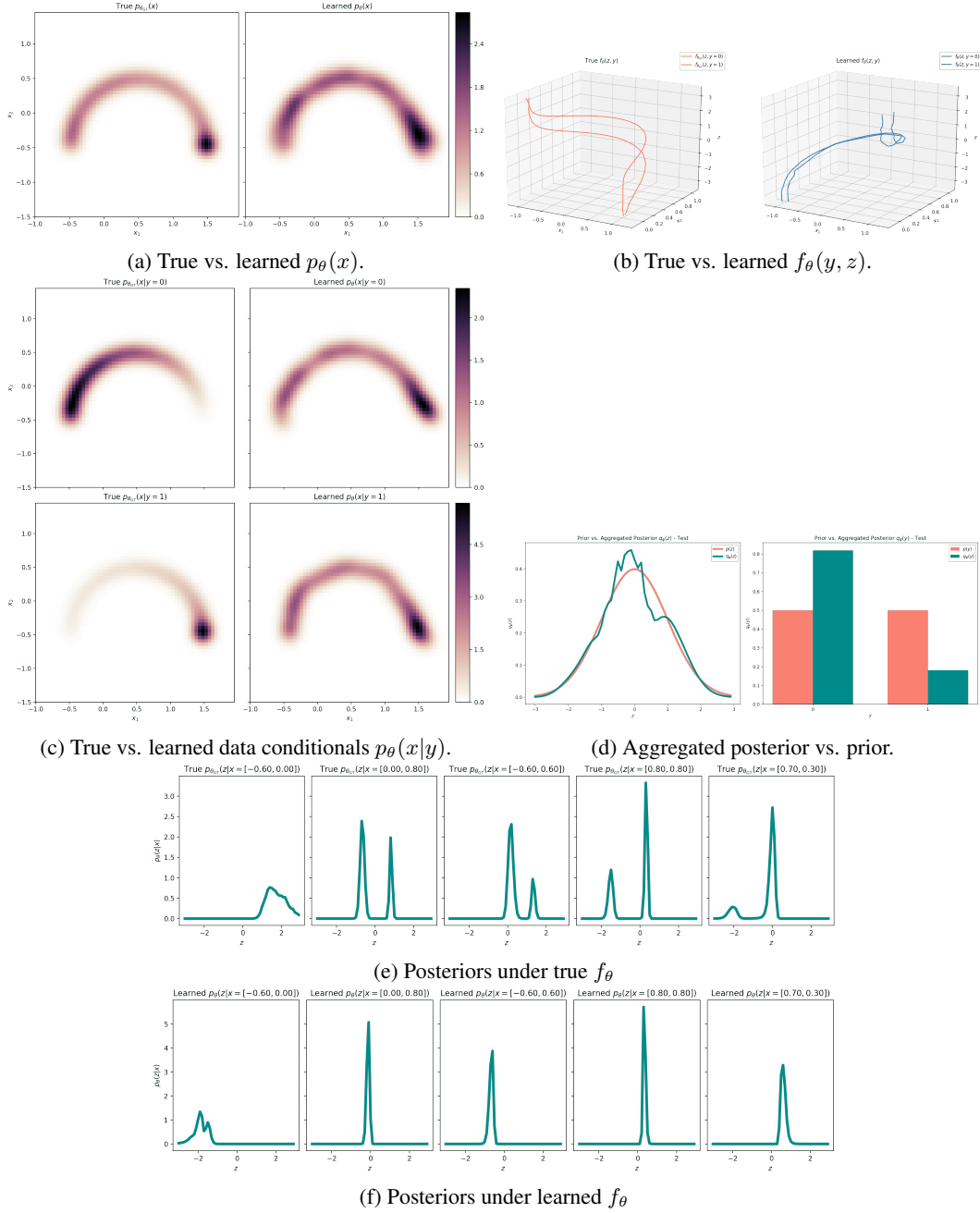


Figure 13: Semi-Supervised MFG-VAE trained on the Discrete Semi-Circle Example. While using semi-supervision, a VAE is still able to learn the $p(x)$ relatively well. However, in this example, given x there is uncertainty as to whether it was generated from $f_\theta(y = 0, z)$ or from $f_\theta(y = 1, z)$, the posterior $p_\theta(z|x)$ is bimodal and will cause a high posterior matching objective. Since semi-supervised VAE objective prefers models with simpler posteriors, the VAE learns a unimodal posterior by collapsing $f_\theta(y = 0, z) = f_\theta(y = 1, z)$, causing $p(x|y = 0) \approx p(x|y = 1) \approx p(x)$. The learned model will therefore generate poor sample quality counterfactuals.

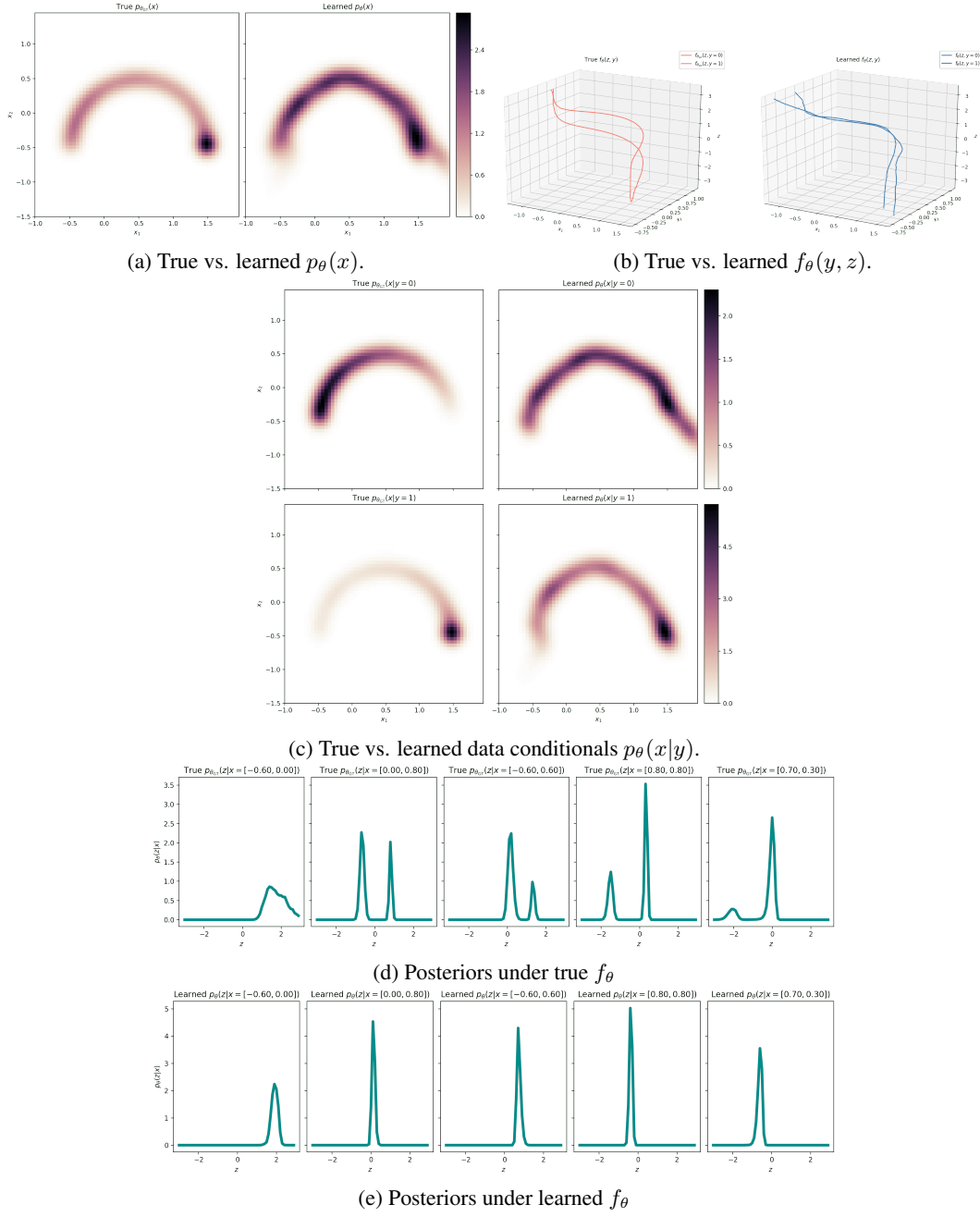
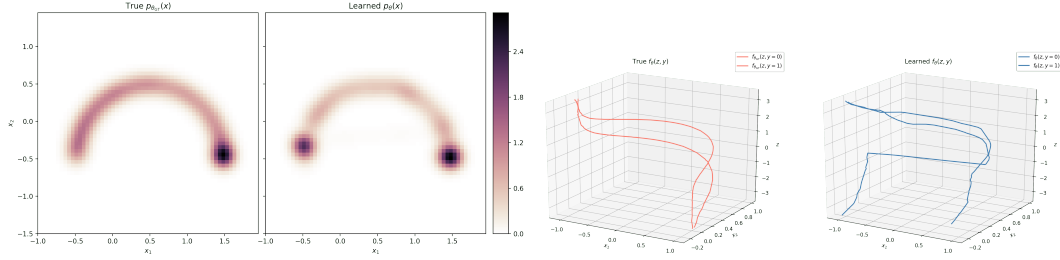
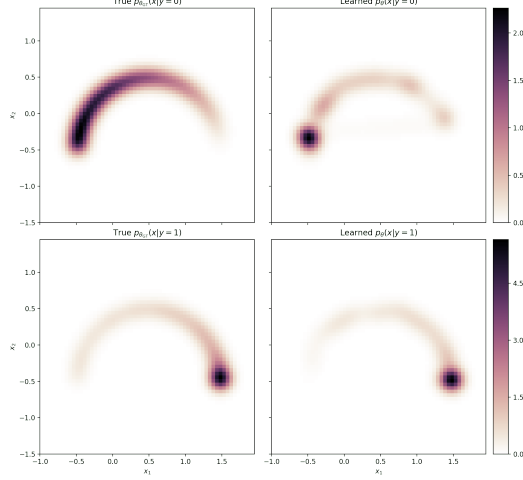


Figure 14: Semi-Supervised VAE trained with Lagging Inference Networks (LIN) trained on the Discrete Semi-Circle Example. While LIN may help escape local optima, on this data, the training objective is still biased away from learning the true data distribution. As such, LIN fails in the same way a MFG-VAE does (see Figure 13).

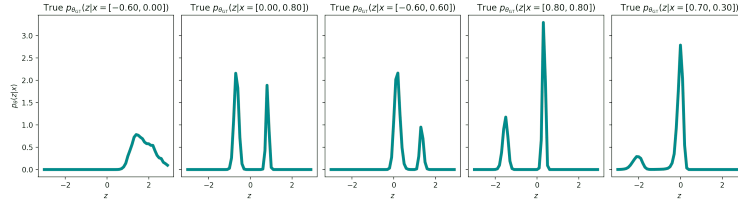


(a) True vs. learned $p_{\theta}(x)$.

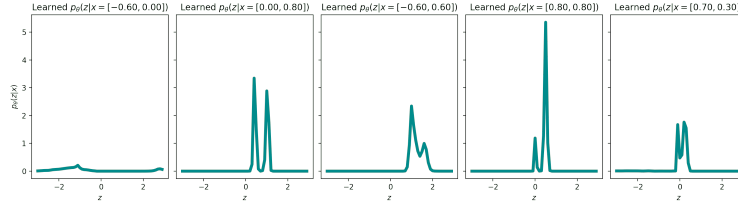
(b) True vs. learned $f_{\theta}(y, z)$.



(c) True vs. learned data conditionals $p_{\theta}(x|y)$.



(d) Posteriors under true f_{θ}



(e) Posteriors under learned f_{θ}

Figure 15: Semi-Supervised IWAE trained on the Discrete Semi-Circle Example. While using semi-supervision, a IWAE is still able to learn the $p(x)$ and $p(x|y)$ better than a VAE. This is because it allows for more complicated posteriors and therefore does not collapse $f_{\theta}(y = 0, z) = f_{\theta}(y = 1, z)$. However, since IWAE has a more complex variational family, the variational family no longer regularizes the function f_{θ} . As such, in order to put enough mass on the left-side of the semi-circle, f_{θ} jumps sharply from the right to the left, as opposed to preferring a simpler function such as the ground truth function.

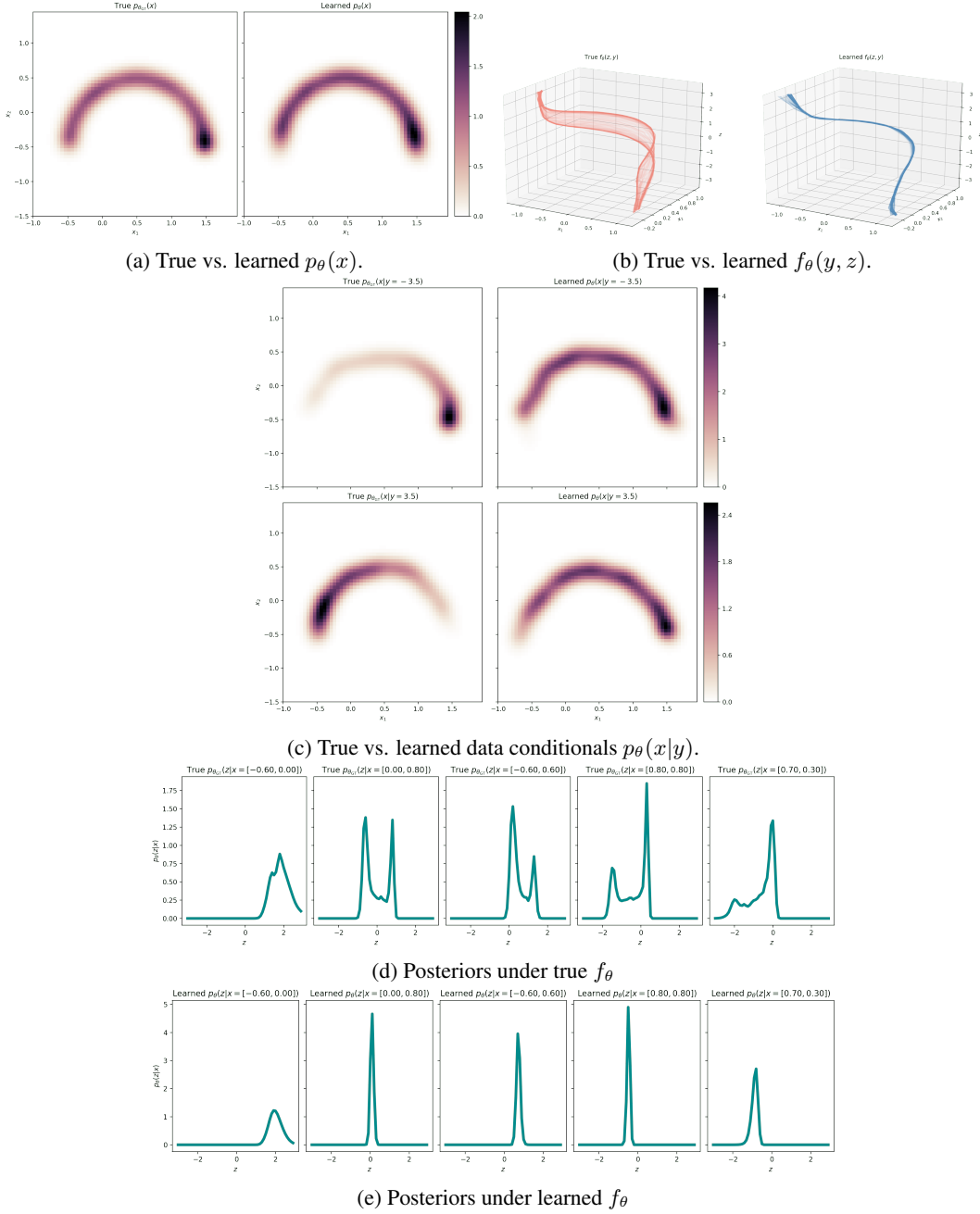


Figure 16: Semi-Supervised MFG-VAE trained on the Continuous Semi-Circle Example. In this example, the VAE exhibits the same problems as in the Discrete Semi-Circle Example (Figure 16). However, with since y is continuous, this poses an additional issue. Since $q_\phi(y|x)$ (the discriminator) in the objective is a Gaussian, and the ground truth $p_\theta(y|x)$ is multi-modal, the objective will select a function f_θ under which $p_\theta(y|x)$ is a MFG. This, again, leads to learning a model in which $f_\theta(y = \cdot, z)$ are the same for all values of y , causing $p(x|y = 0) \approx p(x|y = 1) \approx p(x)$. The learned model will therefore generate poor sample quality counterfactuals.

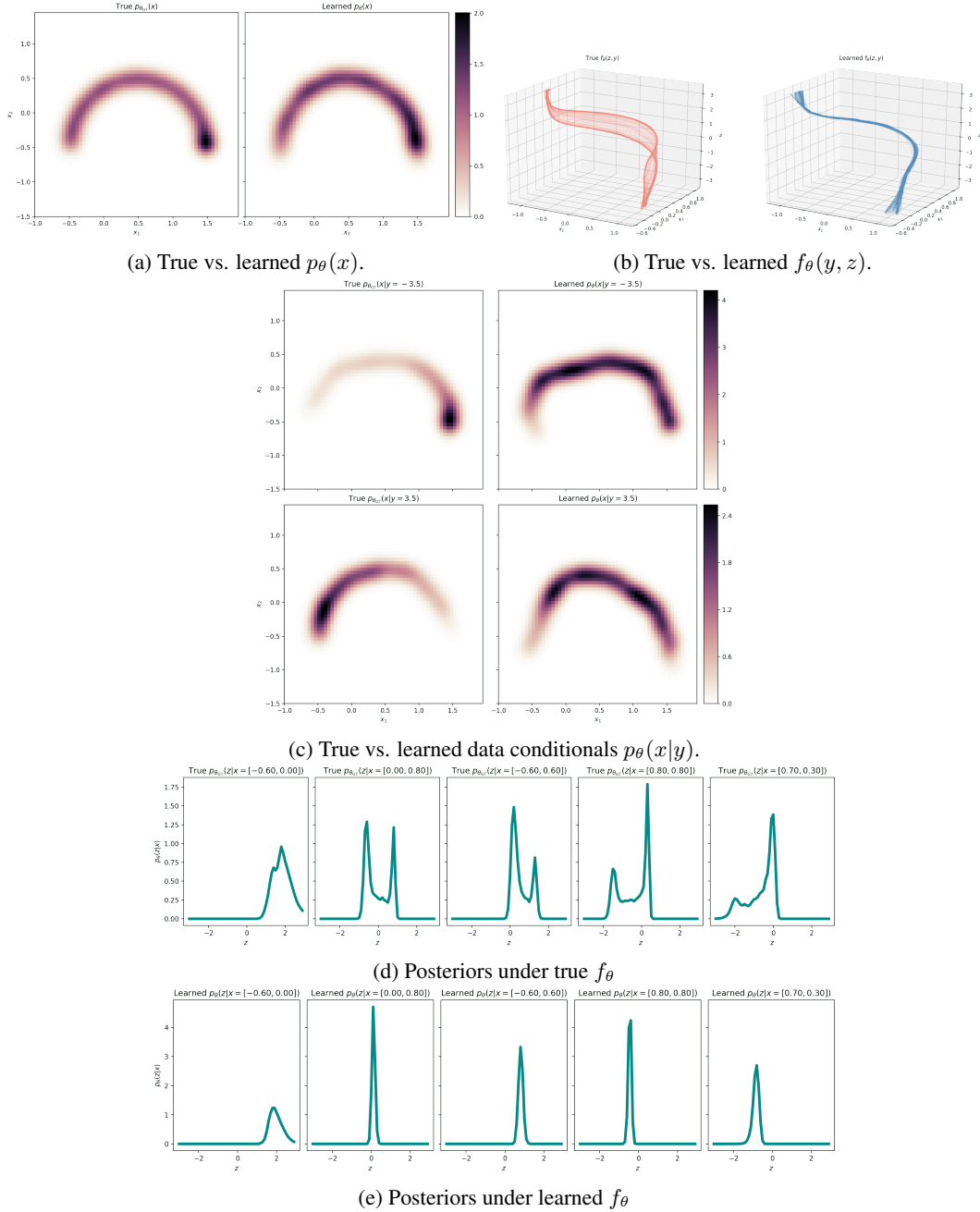


Figure 17: Semi-Supervised VAE trained with Lagging Inference Networks (LIN) trained on the Continuous Semi-Circle Example. While LIN may help escape local optima, on this data, the training objective is still biased away from learning the true data distribution. As such, LIN fails in the same way a MFG-VAE does (see Figure 16).

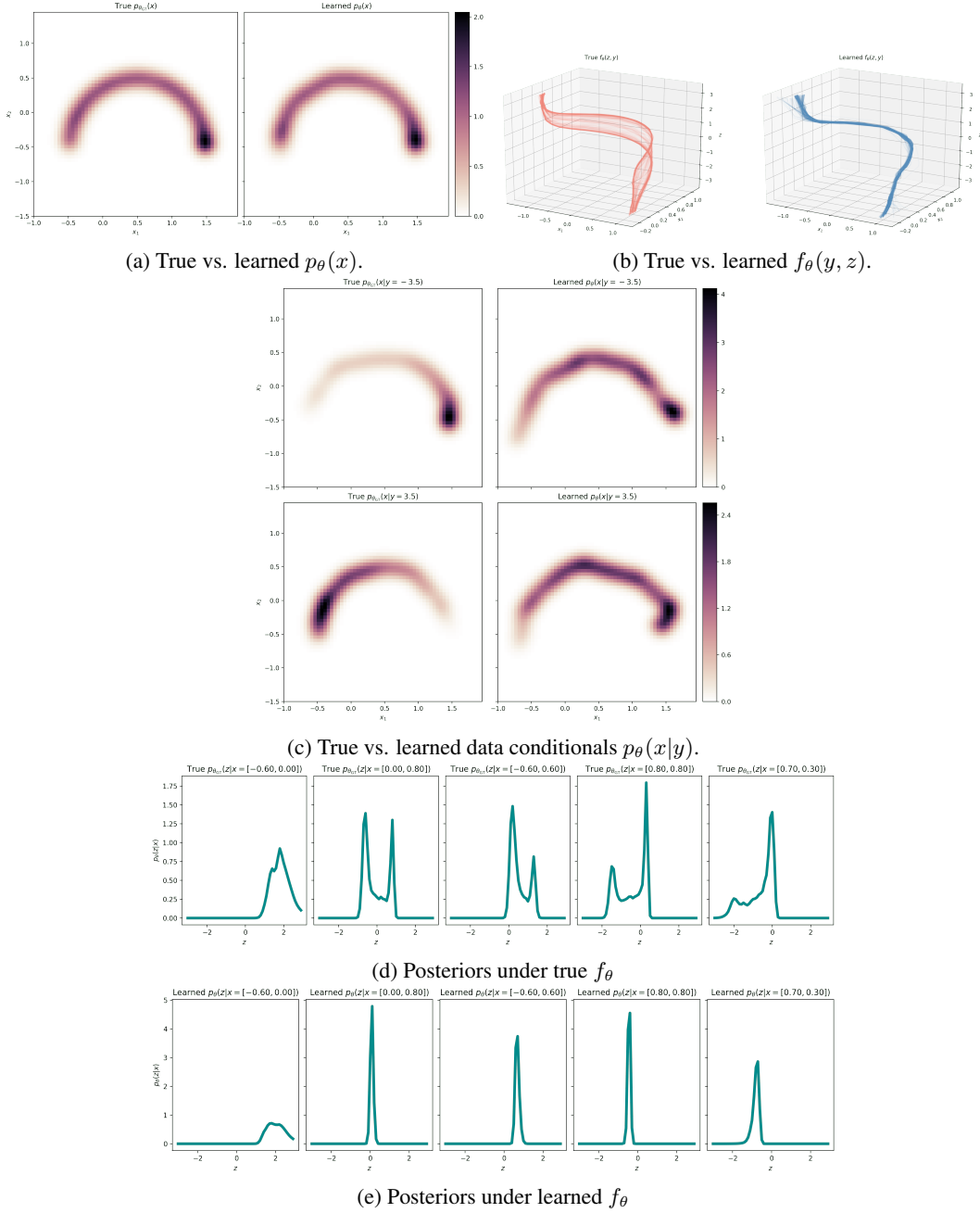


Figure 18: Semi-Supervised IWAE trained on the Continuous Semi-Circle Example. While using semi-supervision, a IWAE is still able to learn the $p(x)$ and $p(x|y)$ better than a VAE. However, since $q_\phi(y|x)$ (the discriminator) in the objective is a Gaussian, and the ground truth $p_\theta(y|x)$ is multi-modal, the objective will select a function f_θ under which $p_\theta(y|x)$ is a MFG. This, again, leads to learning a model in which $f_\theta(y = \cdot, z)$ are the same for all values of y , causing $p(x|y = 0) \approx p(x|y = 1) \approx p(x)$. The learned model will therefore generate poor sample quality counterfactuals.

H.4 When learning compressed representations, posterior is simpler for mismatched models

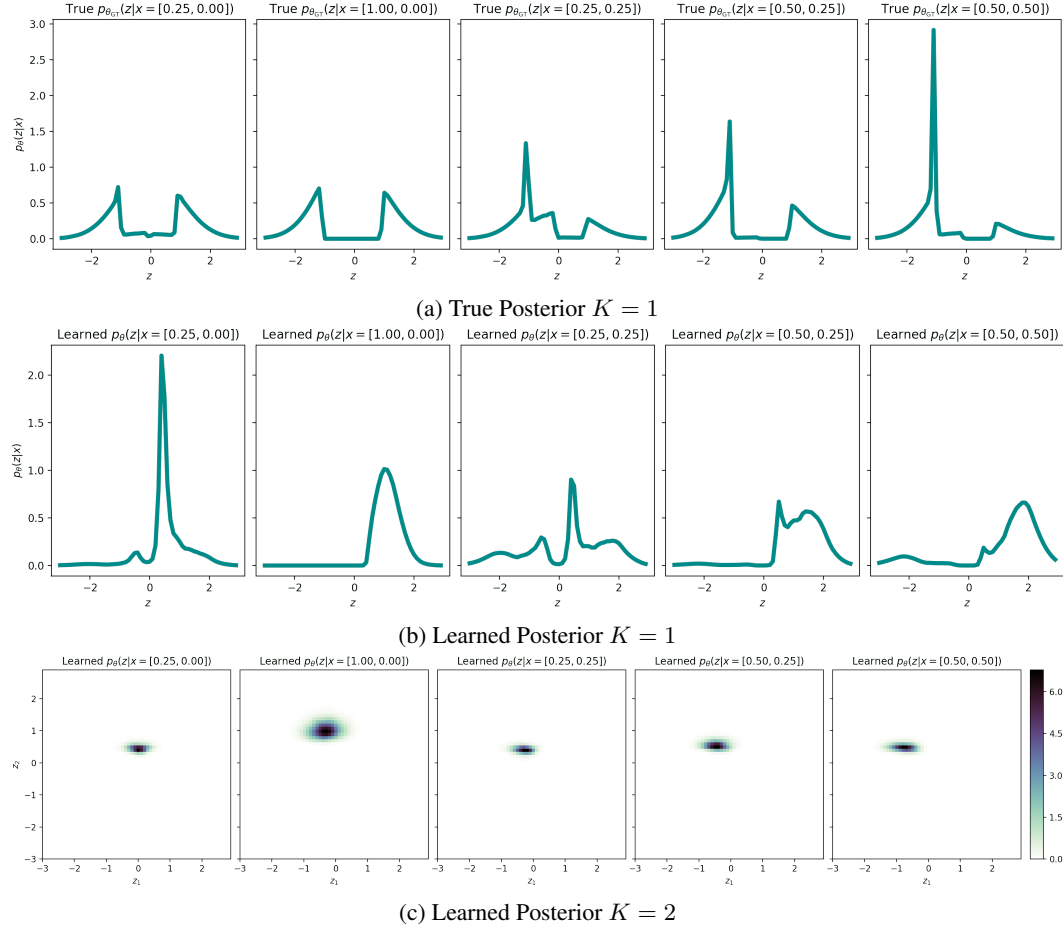


Figure 19: VAEs learn simpler posteriors as latent dimensionality K increases and as the observation noise σ_ϵ^2 decreases on “Clusters Example” (projected into 5D space).

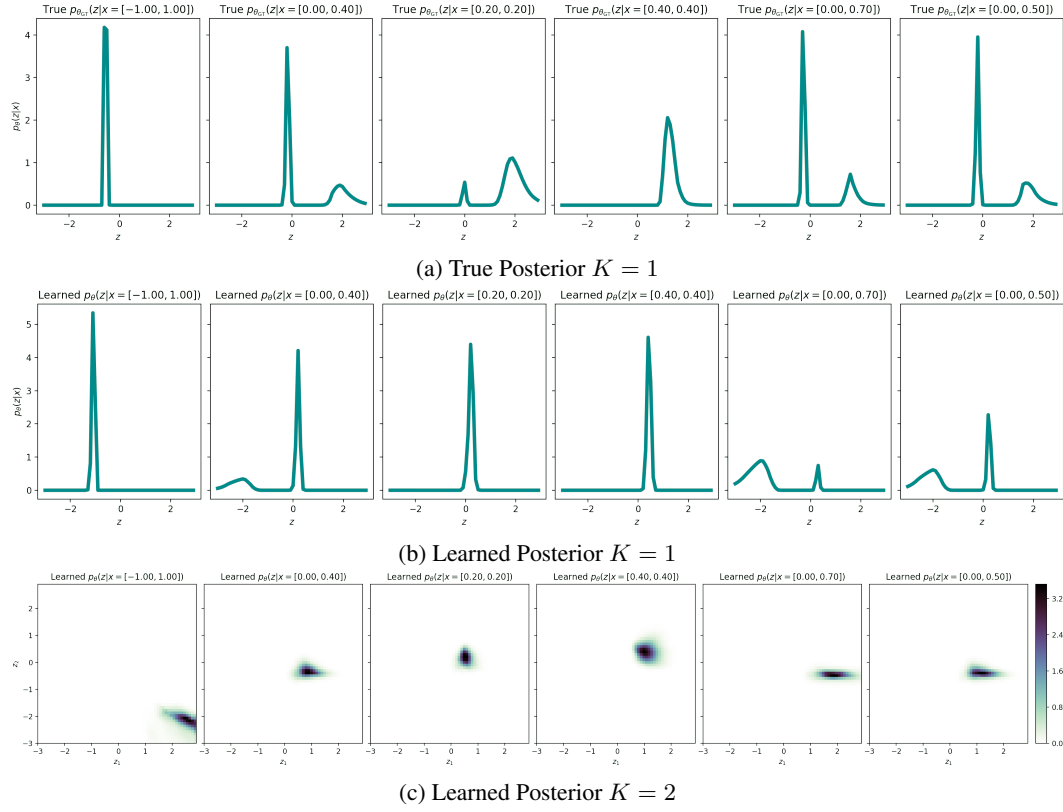


Figure 20: VAEs learn simpler posteriors as latent dimensionality K increases and as the observation noise σ_ϵ^2 decreases on “Figure-8 Example” (projected into 5D space).